

www.acsanm.org Spotlight on Applications

Emerging Applications of Nanoporous Molecular Crystals

Alexandra Robles and Ognjen Š. Miljanić*



Cite This: ACS Appl. Nano Mater. 2023, 6, 15331-15346

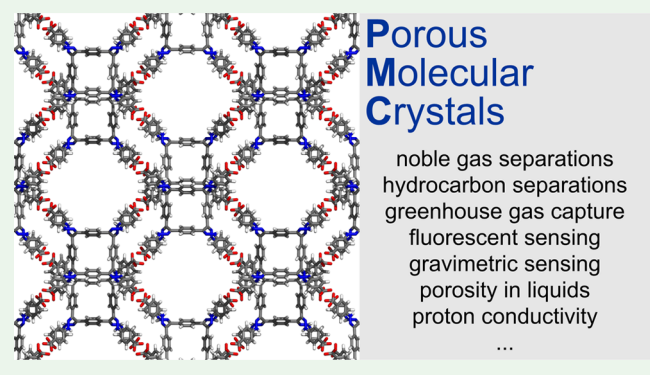


ACCESS I

III Metrics & More

Article Recommendations

ABSTRACT: Porous molecular crystals (PMCs) are a class of nanoporous materials composed of discrete, typically organic molecules held together by noncovalent interactions. While they parallel crystalline polymeric porous materials—zeolites, metalorganic frameworks (MOFs), and covalent organic frameworks (COFs)—in many of their characteristics, they are also distinctly solution- and vapor-processable, offering better possibilities for incorporation into devices and open unexplored frontiers in the creation of porous liquids. In this Spotlight, we will review and examine the examples of emerging applications of PMCs in gas storage and separations, analytical chemistry, the development of porous liquids, and other fields.



KEYWORDS: porous molecular crystals, cages, hydrogen bonded organic frameworks, gas storage, separation, porous liquids

1. INTRODUCTION

Studies and applications of nanoporous materials are in their Golden Age, with hundreds of research groups around the world approaching these topics from the vantage points of material science and chemistry. Among the nanoporous materials, porous molecular crystals (PMCs) stand out because they are constructed from discrete molecules held together in the solid state only by noncovalent interactions such as $\pi \cdots \pi$ stacking, hydrogen bonding, or halogen bonding. While individually weak, such noncovalent forces can act synergistically to produce robust and practical materials. From the pioneering studies by Wuest and co-workers, the chemistry of PMCs has expanded dramatically in the past two decades. PMCs can be divided into intrinsically and extrinsically porous ones.2 The former are constructed from molecules endowed with an internal pore, typically in the form of a central cavity of a shape-persistent macrocycle or cage. The latter is formed by the inefficient solid-state packing of molecules lacking an internal pore. Both have advantages and disadvantages. Extrinsic PMCs are notoriously polymorphous, with the most stable polymorphs typically lacking porosity, making a priori predictions of their packing difficult. On the other hand, the most common classes of intrinsic PMCs are based on the hydrolytically labile imine and boroxine linkages, hindering their applications in practical moisture-rich environments. The chemistry of PMCs has been extensively reviewed by us⁵ and others⁶⁻⁵ with the focus on their connectivity, 10 design, and synthetic approaches. We will aim to not duplicate those previous surveys, and the reader is referred to them for other aspects of PMC chemistry. In this Spotlight, focus will instead be on the emerging applications of this class of porous

materials in the fields ranging from gas storage, 11 separations, and molecular sieving, through their analytical applications, and finally to the new frontiers in proton conduction and the preparation of porous liquids.

2. GAS SEPARATIONS

2.1. Noble Gases. Separations of noble gases present economic opportunities for nuclear, medical, and aerospace industries and remediation challenges on account of toxicity of their radioactive isotopes. The adsorption of argon (Ar), xenon (Xe), krypton (Kr), and radon (Rn) from air is difficult because of their low concentrations. The most abundant argon makes up ~1% of air, while xenon and krypton exist in much lower concentrations of 0.087 and 1.14 ppm by volume (ppmv), respectively.¹² Radioactive radon is a group 1 carcinogen, with its main isotope ²²²Rn occurring naturally with activities up to 15 Bq m⁻³. Radioisotopes of other noble gases, such as 85Kr and 133Xe, are produced during nuclear fission and can enter the atmosphere during nuclear accidents. Efficient separation of noble gases is challenging not only because of their low concentrations and chemical inactivity but also on account of the similarities in their atomic diameter (Ar:

Received: May 16, 2023 Accepted: August 23, 2023 Published: August 29, 2023





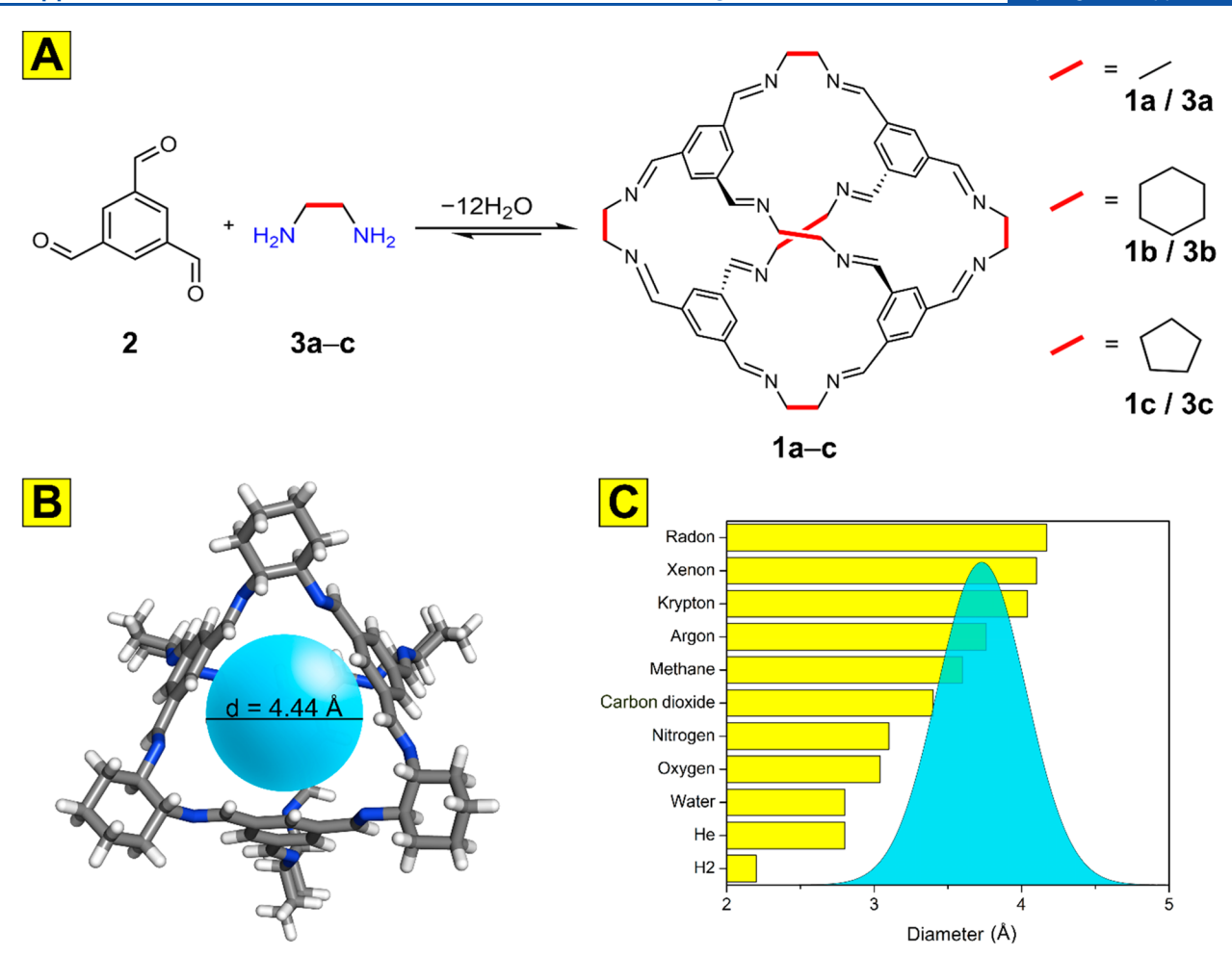


Figure 1. (A) Synthesis of imine cages CC1 (1a), CC3 (1b), and CC4 (1c) via one-pot [4 + 6] cycloimination between trialdehyde 2 and diamines 3a-c. (B) The largest inclusion sphere (aqua) inside cage 1b creates a (C) pore-limiting envelope (aqua) between 3 and 5 Å in crystalline 1b, which encompasses the diameters of several gases with dimensions up to radon; calculated through molecular dynamic simulations. Element colors: C—gray, H—white, N—blue.

3.76 Å, Kr: 3.69 Å, Xe: 4.10 Å, Rn: 4.17 Å), requiring excellent selectivity. ¹⁴

The separation of krypton from xenon and radon has been demonstrated by Cooper et al. within the porous organic cage (POC) 1b, 15 constructed by a [4+6] cycloimination of 1,3,5-triformylbenzene (2) and (\pm)-trans-1,2-diaminocyclohexane (3b, Figure 1A). 16 The intrinsic cavity of 1b can accommodate guests with diameters of up to 4.44 Å (Figure 1B and C), but its packing creates channels with unimodal limiting window apertures of 3.6 Å, which are too narrow for the diffusion of Kr. Interestingly, the gate-opening behavior of the POCs allows for the opportunistic hopping of the large Xe and Rn molecules through the pores. The size match up of Xe within the cavity spaces enhances its selectivity compared to Kr, with Xe having a zero-coverage $Q_{\rm st}$ of 31.3 kJ mol $^{-1}$ vs 23.1 kJ mol $^{-1}$ for Kr.

In breakthrough experiments using a 1:10 Kr/Xe gas mixture, **1b** showed high retention of Xe (11 mmol kg⁻¹, eluting at 15 min) and an ideal adsorbed solution theory (IAST) selectivity of 20.4, 3-fold higher than that of the best performing metal—organic framework, Ni/DOBDC.⁶

Similar Xr/Kr gas separation performance was reported by Chen and co-workers using HOF-40,¹⁷ a doubly interpenetrated permanently porous 3D framework constructed by the self-assembly of 1,2,4,5-tetrakis(4-cyanophenyl)-benzene. Whereby the selectivity of Xe in 1b depended on

size-exclusion molecular sieving, the higher binding affinity for Xe over Kr in the 1D channels of HOF-40 is assisted by multiple Xe···H van der Waals interactions between each Xe molecule and eight neighboring benzene rings. This observation is consistent with a strong absorption of Xe (zero coverage $Q_{\rm st}$ of 32.8 kJ mol⁻¹) over Kr ($Q_{\rm st}$ = 24.4 kJ mol⁻¹). The IAST selectivity value of Xe/Kr in a binary gas (20/80) gas mixture under 289 K and 1 bar was calculated to be 11.2, lower than that of 1b under similar conditions (12.5), but higher than other HOFs¹⁸ and POCs. ^{19,20} Later computational studies by Jelfs and co-workers²⁰ compared guest-binding energies for POCs, cucurbiturils, cyclodextrins, and cryptophanes, and confirmed 1b as the most promising material for Xe/Kr separations.

Solution processability of **1b** allowed Carreon and coworkers to deposit it as a membrane material for the efficient separation of Xe from light gases such as helium (He), CO₂, Kr, and CH₄. The crystals of **1b** were seeded onto bare alumina tubes, which were then treated solvothermally at 50–120 °C for up to 60 h, forming a 2.5 μ m-thick coating on the supports. SEM images showed a tightly packed coating with continuous size distribution of octahedral crystals with dimensions of 1.04 \pm 0.14 μ m, confirming the high-quality of membranes produced by this approach. Gas permeation studies were done at a flow rate of 100 SSMs using feed and

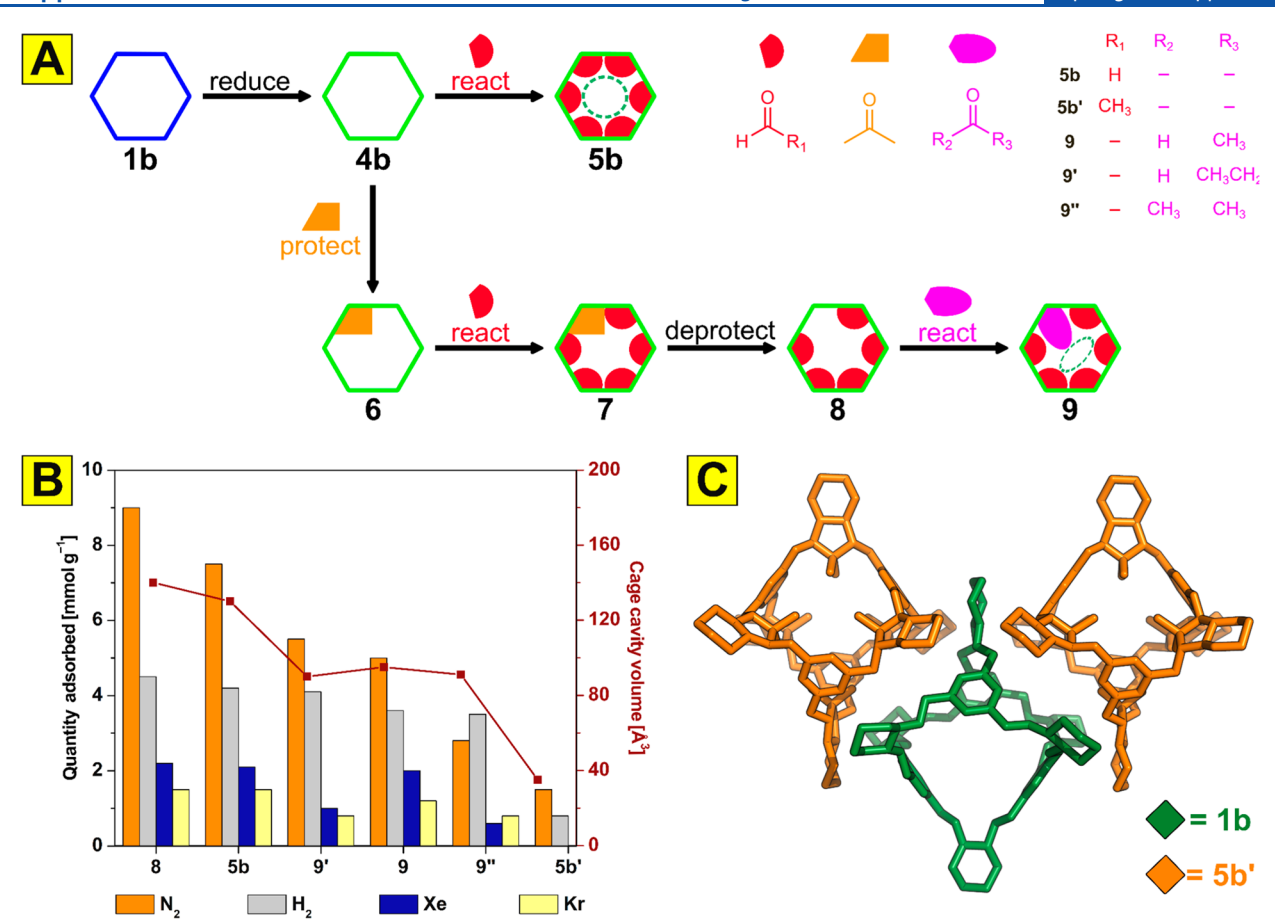


Figure 2. (A) Systematic strategy was used to tune the cavity size (shown by the dotted green line) of cages 5b and 9. (B) Gas sorption properties (left side axis; histogram) and cage cavity volumes (right axis) of the functionalized cages. (C) Co-crystal of 1b and 5b' in a 1:1 ratio was made to integrate capacity and selectivity in a single material; hydrogens are omitted for clarity. Adapted with permission from ref 22. Copyright 2019, AAAS.

transmembrane pressures of 223 and 138 kPa, respectively. This system had moderate selectivities for light gases over xenon ranging from 2.2–13 but showed a high gas permeances of 2114, 1705, 773, and 1962 gas permeance units (GPUs) for He, CO₂, Kr, and CH₄, successively. These membranes show promise for extracting Xe from air sources and demonstrate the feasibility of PMCs' incorporation into devices for industrially relevant separations.

2.2. Hydrogen Isotopes. Another separation of relevance to the nuclear industries is that of hydrogen isotopes. Very small dimensions of protium and deuterium molecules require very small pore apertures (~3 Å) for selective kinetic sieving, in turn slowing their transport and decreasing the overall adsorption capacities for both isotopes. Cooper et al. 22 offered a solution to this problem by postsynthetically modifying the reduced cage 4b through functionalization of the six internal diamine moieties with formaldehyde and other carbonyl compounds (Figure 2A). As seen on the right-side axis of Figure 2B, this strategy allowed fine-tuning of the internal cage cavity without affecting the overall crystal packing. While some selectivity could be accomplished, the best results were obtained in a 1:1 cocrystal system of the nonfunctionalized cage 1b and the internally decorated 5b' (Figure 2C). The internally functionalized 5b' acted as a H2 diffusion blocker, while the "empty" 1b allowed the inclusion of large amounts of D₂ into the pores. The cocrystal showed an 8:1 selectivity for D_2 over H_2 , and a high D_2 uptake of ~ 4 mmol g^{-1} .

In a subsequent study, Marken and co-workers examined the effects of pH on this separation performed on a Pt electrode surface. They observed a decrease in H₂ binding within **1b** on lowering the pH from 8 to 6, suggesting that the rate of adsorption/desorption could be tuned by using a buffer electrolyte solution. The uptake and release of hydrogen gas also appeared to be coupled to water release and uptake, respectively, showing that an aqueous electrolyte solution could be employed to enhance the capture of hydrogen for energy storage applications.

2.3. Hydrocarbons. The challenge of separating gas mixtures containing components of similar shapes, sizes, and volatilities is also prevalent in the separation of hydrocarbons. Industrial separation of light hydrocarbons such as methane (CH_4) , ethane (C_2H_6) , acetylene (C_2H_2) , ethylene (C_2H_4) , propylene (C₃H₆), and propane (C₃H₈) depend on energyintensive cryogenic distillations. However, the flexibility, pore tailoring, and solution processability of PMCs provide new possibilities to produce membranes capable of achieving these challenging separations with much lower energy costs. Chen and co-workers developed and studied several hydrogenbonded organic frameworks (HOFs) capable of strong and selective binding of specific hydrocarbons. Their initial studies focused on two microporous structures—HOF-1, derived from the C_4 -symmetric tetrakis(4-bromophenyl)methane, ²⁴ and HOF-16, derived from the C_3 -symmetric tris(4carboxyphenyl)amine)²⁵ that served as excellent platforms

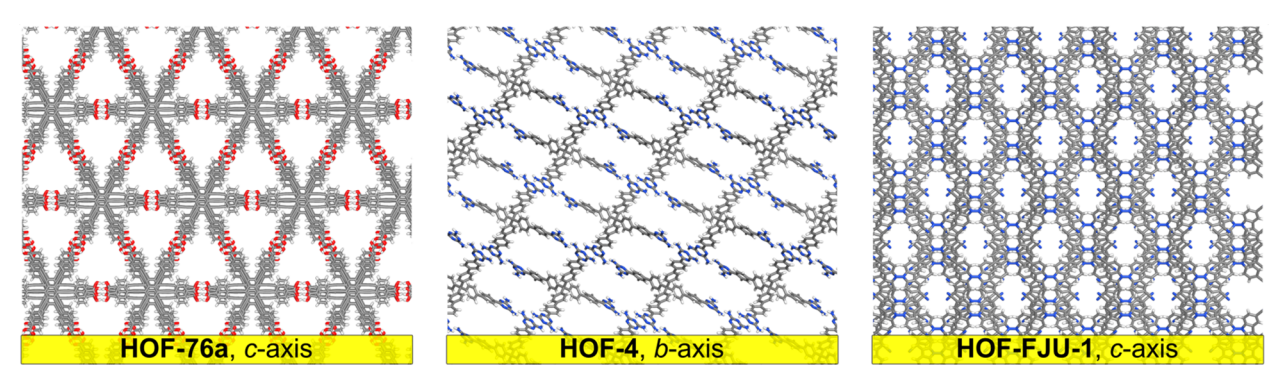


Figure 3. Hydrogen bonded frameworks with tuned pore shapes and sizes are used for selective hydrocarbon capture. Element colors: C—gray, H—white, N—blue, O—red.

for C_2H_2/C_2H_4 and C_3H_6/C_3H_8 separations, respectively. HOF-1 self-assembles into an 8-connected three-dimensional (3D) network with square one-dimensional (1D) channels and cavities with a diameter of 8.2 Å. This report was the first example of a robust HOF that maintained its crystallinity after solvent removal and exhibited moderately high permanent porosity with a Brunauer–Emmett–Teller (BET) surface area of 359 m² g⁻¹. The selectivity of HOF-1 for C_2H_2 over C_2H_4 can be explained by its narrow pores and the interaction between acetylene's acidic hydrogens and the basic amine sites of HOF-1. In the case of HOF-16, the affinity for propylene arises from the unique pore structure and the polarity of the free –COOH moieties lining the 1D channels, which engage in strong interactions with C_3H_6 . Propylene is favored over propane by a factor of 5.4.

For the separation of ethane from ethylene, Chen and coworkers have reported three hydrogen-bonded organic frameworks: HOF-76a,²⁶ HOF-4,²⁷ and HOF-FJU-1a (Figure 3).²⁸ To achieve selective capture of C₂H₆, they focused on tuning the size and shape of the pores in HOF-76a to better match the nonplanar structure of C₂H₆ over that of the planar C₂H₄ molecules. By using the C_6 -symmetric hexakis(4-carboxyphenylethynyl)benzene, triangular 1D channels were constructed to engage in multipoint van der Waals interactions with ethane. This material demonstrated twofold selectivity for C₂H₆ over C₂H₄, the highest by a HOF to date. To in turn favor ethylene over ethane, they investigated the effect of channel confinement in HOF-4 through interpenetration to control the favored uptake of C2H4. Later studies focused on HOF-FJU-1a, a microporous material derived from the C2symmetric 3,3',6,6'-tetracyano-9,9'-bicarbazole, to exclusively capture C₂H₄. The uptake of C₂H₄ within HOF-FJU-1a was tested in C_2H_4/C_2H_6 separations as well as against a $H_2/$ $C_3H_6/CH_4/C_3H_8/C_2H_6/C_2H_4$ gas mixture with high success. The selectivity for ethylene in the equimolar mixture of C_2H_4 / C₂H₆ could be tuned by changes in temperature and ranged from 10.5 to 42.3. In comparison to the selectivity of 14 reported for HOF-4, the excellent performance of HOF-FJU-1a can be attributed to its compact structure minimizing hydrogen bonding interactions, strong intermolecular $C-H\cdots\pi$ interactions between the gas molecules, and the high basicity of the cyano groups.

Intrinsically porous structures such as POCs or cavitands have recently been used for gas separations, on account of the difficulties associated with activating HOFs. Yuan and coworkers have reported two concave calix[4]resorcinarene-based structures that are easy to functionalize around the rim

while maintaining fourfold symmetry. The first of these was a truncated octahedral calix[4]resorcinarene-based POC, CPOC-301, ²⁹ that exhibited strong π -complexation with ethylene, affording a low selectivity of <1.4 over ethane, comparable to those reported by the [4 + 6] boronic ester cage by Mastalerz et al. ³⁰ More recently, Yuan et al. reported CPOC-101 (10), ³¹ a [2 + 4] dimeric lantern-shaped POC self-assembled from tetraformyl-functionalized calix[4]-resorcinarene vertexes (11) and 1,3-diaminopropane (12) linkers (Figure 4A). Multiple solid-state packing patterns were

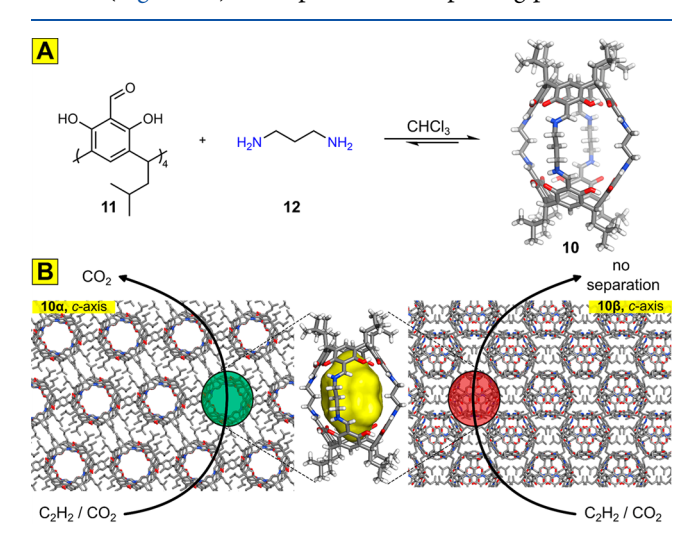


Figure 4. (A) Synthesis of CPOC-101 (10) via [2 + 4] cycloimination of tetraaldehyde 11 and diamine 12. (B) Solvomorph 10α packs to create 1D channels capable of C_2H_2/CO_2 separation (left), while solvomorph 10β has a tightly packed framework unable to separate the two gases. Solvent accessible space within the cavity of 10 is shown in yellow. Element colors: C—gray, H—white, N—blue, O—red.

observed for 10 depending on the recrystallization solvents—CHCl₃ and PhMe yielded 10α (Figure 4B left), which packs to form 1D channels along the *c*-axis, and PhNO₂, PhEt, PhCH=CH₂, PhMe₂, and PhCl produced solvomorphs 10β , 10γ , 10ε , 10δ , 10ζ , 10η , and 10θ , respectively, which all pack in a window-to-vertex fashion (Figure 4B, right) with no channels present in the frameworks and BET surface areas below $40 \text{ m}^2 \text{ g}^{-1}$.

The permanent porosity of 10α was confirmed through gas sorption experiments, which showed the activated framework had a BET surface area of 406 m² g⁻¹, the highest among all the solvomorphs, and a C_2H_2 uptake capacity of 95.02 cm³ g⁻¹

at 298 K and 1 bar, 50% higher than that for CO_2 (63 cm³ g⁻¹). The affinity toward C_2H_2 was confirmed through the measurements of the isosteric heat of adsorption and DFT calculations which found that acetylene molecules interact with the host via $C \equiv C - H \cdots O/\pi$ interactions that are stronger than the hydrogen bonding interactions of the CO_2 molecules residing outside of the cage windows. The IAST selectivity in C_2H_2/CO_2 gas separations was calculated to be 11.9 at 298 K and 100 kPa in an equimolar gas mixture, 14-times lower than that of HOF-3a.³² Though exhibiting lower selectivities than the extrinsically porous PMCs, POCs maintain the advantage of more accessible permanent porosities vs the weakly held together HOFs. This pioneering work demonstrates how polymorphism can be used to tailor the gas sorption and separation abilities of POCs.

Another approach to tailor the void spaces of POCs was demonstrated by Bloch and co-workers, 33 who reported that N_2 flow activation at 250 °C of the octahedral imine-based porous organic **1b** affords a desolvated framework, **1\beta**, with a BET surface area of 652 m² g⁻¹. This β -form of the cage shows high low-pressure gas uptake capacities for C_2H_n/CH_4 separations, with the adsorption enthalpies for methane (-23 kJ mol⁻¹), ethylene (-32 kJ mol⁻¹), acetylene (-33 kJ mol⁻¹), and ethane (-35 kJ mol⁻¹) being comparable to those of other PMCs. The high adsorption enthalpy for ethane was attributed to optimal pore size, highlighting how the molecular nature and structure of POCs enables postsynthetic densification and affect adsorption behaviors.

Multiple computational studies have explored other avenues to enhance gas uptake selectivities by POCs. Jelfs et al. 34 explored the mechanism of gas sorption behavior in multicomponent PMC $1a\cdot 1b_n\cdot 1c_{1-n}$ composed of Cooper's imine cages. These systems were further explored by Doonan and co-workers who used Voronoi network analysis and center of mass radial distribution functions to predict new robust amorphous solids, with higher gas storage capacities. 36

2.4. Greenhouse Gas Capture. Small amounts of water vapor (H₂O), carbon dioxide (CO₂), methane (CH₄), and nitrous oxide (NO₂) in the atmosphere cause the Earth's natural greenhouse effect. However, human activities are increasing the atmospheric concentrations of greenhouse gases, leading to a rapid (on a geological time scale) increase in the average global surface temperatures. Gases such as hydrofluorocarbons (HFCs), perfluorocarbons (PFCs), sulfur hexafluoride (SF₆), CO₂, and CH₄ have large global warming potentials (GWPs). Other culprits accumulate in single layers of the atmosphere: carbon monoxide (CO), sulfur dioxide (SO₂), and volatile organic compounds (VOCs) in the troposphere and hydrochlorofluorocarbons (HCFC) and chlorofluorocarbons (CFCs) in the stratosphere, where they contribute to ozone depletion. Pioneering studies of the adsorption of potent greenhouse gases in PMCs were done by Atwood in the early 2000s.³³

Much recent work on ambient air pollutants has focused on tropospheric aerosols, such as SO₂. Cooper and co-workers reported the study of three structurally related *N*-containing functional cages: **1b** (imine), **4b** (secondary amine), and **5b** (tertiary amine) which exhibited SO₂ capacities of 2.78 mmol g⁻¹, 12.34 mmol g⁻¹, and 13.78 mmol g⁻¹, successively.³⁸ The amine groups in **5b** strongly interact with SO₂ to draw more molecules into its intrinsic void than **1b** (Figure 5, top), but **1b** cannot be easily regenerated on account of its high binding affinity of 82.78 kJ mol⁻¹ (Figure 5, middle). In contrast, the

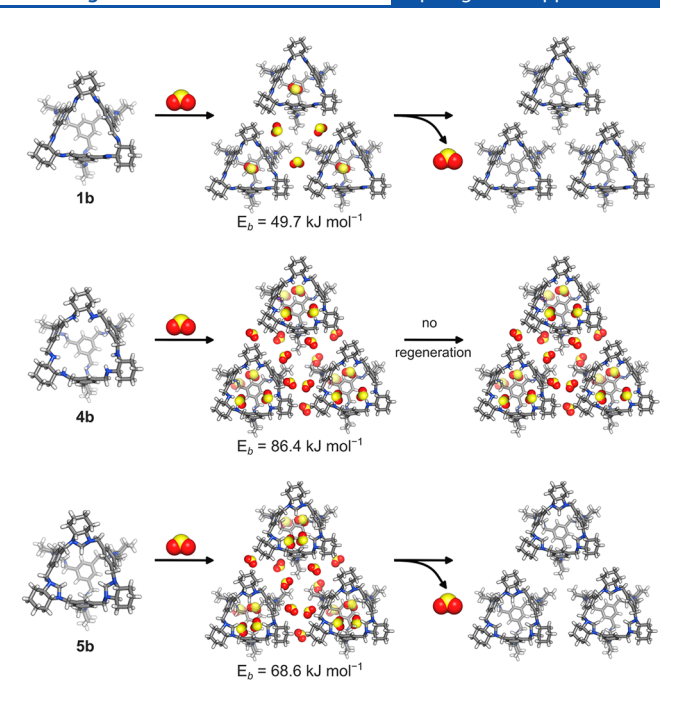


Figure 5. Sorption behavior of porous cages 1b (top), 4b (middle), and 5b (bottom) in the presence of SO_2 as the guest. Element colors: C—gray, H—white, N—blue, O—red, S—yellow. Adapted with permission from ref 38. Copyright 2021, Wiley.

imidazolidine rings on $\bf 5b$ seem to have an ideal affinity for $\rm SO_2$ at 43.03 kJ mol⁻¹; this middle-of-the-road value allows large amounts of $\rm SO_2$ molecules to enter the cage while still being able to be evacuated under a dynamic vacuum at 80 °C (Figure 5, bottom). The uptake by $\bf 5b$ rivaled those of MOFs, which, however, cannot be easily regenerated for cycling of the adsorbent due to the strong interactions they form with $\bf SO_2$. The high storage density of $\bf 5b$ makes it a promising replacement for the currently employed amine scrubbers as this cage can pack $\bf 12$ amine groups in a small volume, making it better suited for industrial $\bf SO_2$ capture.

While CO₂ is the most abundant greenhouse gas, CFCs have much higher GWPs. Many CFCs have long atmospheric lifetimes-55 years for CFC-11, 140 years for CFC-12, and 640 years for CFC-13—allowing them to reach the stratosphere and cause detrimental ozone depletion. CFCs were previously heavily employed in refrigerants, propellants (HFC-227ea, HFC-225ca), foaming agents (CFC-113), and electronics (CF₄, SF₆, perfluorohexane). Though the manufacturing of some of them was banned under the Montreal Protocol, replacement hydrofluorocarbons still have high GWPs. Thus, the capture and sequestration of these fluorinated pollutants is of significant interest. Our group reported³⁹ trispyrazole 13 (Figure 6A) that self-assembles into an extended framework via six N-H···N hydrogen bonds that create hexagonal 1D channels and six $\pi \cdots \pi$ stacking arrangements between the electron-poor pyrazole moieties and the electron-rich tetrafluorobenzenes (Figure 6B) that form the 3D framework. The fluorine-lined hexagonal voids measure 16.5 Å in length (Figure 6C), and the activated framework has a BET surface area of 1159 $\mathrm{m}^2~\mathrm{g}^{-1}$. The hydrophobic nature of this material was confirmed through water contact angle measurements $(132 \pm 1^{\circ})$ and water vapor sorption experiments, which showed that even at 90% relative humidity (RH), the crystals of 13 took up negligible amounts of water. Further gas sorption

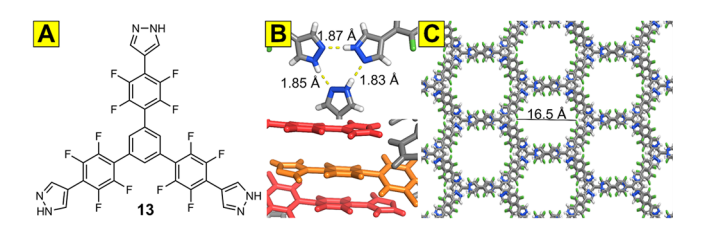


Figure 6. (A) Trispyrazole **13** engages in (B) N-H \cdots N hydrogenbonding (top) and π ··· π stacking (bottom) interactions to create (C) an extrinsic PMC with hexagonal voids 16.5 in width. Element colors: C-gray, H-white, N-blue, F-lime.

experiments used TGA to test the ability of these highly fluorinated materials to adsorb fluorocarbons and CFCs. The adsorption capacities were determined to be 1.58 mol mol⁻¹, 2.52 mol mol⁻¹, and 2.96 mol mol⁻¹ for perfluorohexane (GWP₂₀ of \sim 6,600), Cl₂FC-CClF₂ (CFC-13, GWP₂₀ of \sim 6,540), and CF₃CHF₂CHCl₂ (HCFC-225a, GWP of \sim 429), respectively. Previous reports have shown that such adsorption is possible within fluorinated MOFs based on similar ligands, but unfortunately of inferior stability to ambient conditions. In a subsequent study, we have shown that fluorinated inhalation anesthetics with GWP₂₀ values between 349 and 3714 can also be adsorbed within the pores of 13.41

3714 can also be adsorbed within the pores of 13. 41 In a recent study, 42 Mastalerz's group has shown the critical importance of fluoro substitution of their triptycene-based cages in enhancing the binding capacities for small perfluorocarbons with GWP₁₀₀ values ranging from 6630 to 9540. In moving from cages substituted with butyl to those substituted with perfluorobutyl groups, the molar uptake capacities increase approximately 2-fold for CF₄, 3-fold for C₂F₆, and almost seven times for C₃F₈. Selectivity for the fluorocarbons over nitrogen also increases dramatically in the same series. Sulfur hexafluoride (SF₆) is one of the most detrimental 350 greenhouse gases. Cooper and co-workers reported⁴³ the capture of SF₆ (GWP₁₀₀ of \sim 23,000) using their imine cage 1b. This POC has a high affinity for SF₆ with each cage molecule taking up 2.9 molecules of SF₆ and heat of adsorption reaching 45 kJ mol⁻¹. The IAST selectivity for a 90:10 (v/v) N₂/SF₆ gas mixture under 298 K and 1 bp was calculated to be 74. Breakthrough experiments performed under the same conditions revealed the slow desorption of SF₆, taking about 20 min. Computational studies of this system were performed to further investigate the kinetics of SF₆ adsorption in 1b, and a very slow diffusion, about 4.8 \times 10^{-13} m² s⁻¹ at 335 K, was calculated for the large SF₆ (5.5 Å) molecules in the small cavities of 1b.44 Despite smaller-thanoptimal cage apertures, this cage showed unprecedented separation of this greenhouse gas from nitrogen.

Much work has been done on the capture and separation of the two most common greenhouse gases: carbon dioxide and methane. Mastalerz et al. have studied the adsorption and separation of these two gases in functionalized adamantoid cages based on salicylimine linkages. The BET surface area of cage 14 was calculated to be 1377 m² g⁻¹, which was the highest reported for purely organic porous materials at the time, and its void volume of 0.42 cm³ g⁻¹ is larger than that of 1b (0.28 cm³ g⁻¹). The cage has a CO₂/CH₄ selectivity of 10, and the hydroxy groups positioned inside the cavity assist in the preferential adsorption of carbon dioxide (2.1 mmol g⁻¹) over methane (0.61 mmol g⁻¹) at 237 K and 1 bar. These adsorption capacities are comparable to those of the imine

cages reported by Cooper et al. and exceed the overall uptake by the imine cages synthesized by Zhang and co-workers. ⁴⁶

Chen, Miljanić, and co-workers have also investigated the efficient CO_2 capture by intrinsic PMCs employing cyclotetrabenzoin acetate (17). This permanently porous macrocycle is easily synthesized through the benzoin condensation cyclooligomerization of terephthaldehyde, followed by esterification with acetic anhydride. The crystals of 17 retain their framework after desolvation (Figure 7, left) and have a BET

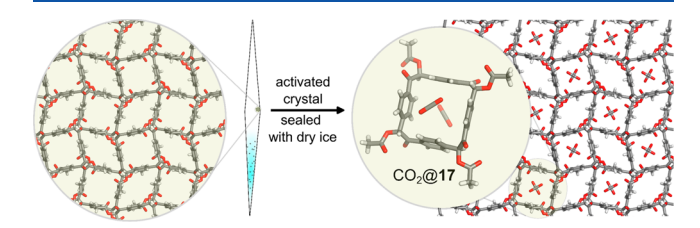


Figure 7. Activated crystal of 17 (left) can be mounted onto a capillary filled with dry ice for the *in situ* SCXRD of CO₂@17 (right). Element colors: C—gray, H—white, O—red.

surface area of 570 $\mathrm{m^2~g^{-1}}$ with a pore volume of 0.18 $\mathrm{cm^3~g^{-1}}$. The polar carbonyl groups point inward toward the square channels, forming an aperture with approximate dimensions of $5.0 \times 5.0 \text{ Å}^2$, which offers kinetic selectivity for CO₂ capture. Gas sorption isotherms reveal a high adsorption of 68 cm³ g⁻¹ for CO₂ compared to those of N₂ and CH₄, 1.6 cm³ g⁻¹ and 9.7 cm³ g⁻¹, respectively. The interaction of CO₂ with the macrocyclic host is confirmed through the zero-coverage Q_{st} of 33.7 kJ mol⁻¹, and in situ single crystal X-ray diffraction (SCXRD) on $CO_2@17$ (Figure 7, right). The structure revealed that the CO2 molecules are stabilized in the cavities of cyclotetrabenzoin acetate by $\pi \cdots \pi$ stacking interactions with the benzene "walls" of 17, which provides thermodynamic control for this preferential adsorption. Breakthrough experiments were conducted on binary gas systems (50:50 CO₂/N₂ or CO_2/CH_4) at 298 K and 1 bar, and both yielded high purity gases in under 50 min. This system can be easily regenerated and remains stable for up to 30 cycles.

Later studies on 17 focused on CO₂/CO gas separation, and high performance was observed for both bulk 50:50 v/v and trace 1:99 v/v gas mixtures. The IAST CO₂/CO selectivities were calculated to be 10.1 for the 50:50 gas mixture and 102 for the 1:99 gas mixture at 298 K and 1 bar. Upon lowering the temperature, the selectivities increased to 16.8 and 166, respectively, proving the strong binding of CO₂ over CO (zero-coverage $Q_{\rm st}=12.9~{\rm kJ~mol^{-1}}$). Both systems can be operated and regenerated at ambient conditions and reduced pressures, without the need for changes in temperature, therefore, proving that intrinsic PMCs are promising platforms for low-cost pressure-swing adsorption (PSA) technologies.

Another example of a permanently porous PMC with higher affinity toward CO_2 over CH_4 and N_2 is HOF-11, ⁴⁹ reported by Chen and co-workers in 2017. This HOF derived from a tricaboxylic organic building unit (OBU), tris(4-carboxyphenyl)amine, engages in dimeric O–H···O hydrogen bonding interactions to create 1D hexagonal apertures with dimensions of $6.2 \times 6.8 \text{ Å}^2$. Layers of these interconnected layers stack on top of one another to create a robust 11-fold interpenetrated 3D framework with a CO_2 -deduced BET surface area of $687 \text{ m}^2 \text{ g}^{-1}$. The activated framework exhibits selectivities of 4.2 and 13.1 for CO_2 over CH_4 (50:50 mixture)

and N_2 (15:85 mixture), respectively, at 296 K and 1 atm, and of 4 and 15.1 from those same mixtures at 273 K. These selectivities, while slightly lower than those for other reported frameworks such as SOF-1a⁵⁰ and HOF-5a,⁵¹ demonstrate the ability of multicarboxylate OBUs to construct robust HOFs for selective gas separations.

To date, there have only been a handful of HOFs whose permanent porosities have been confirmed by gas sorption isotherms. 32,39,50,52 Due to the weak interactions holding the frameworks together, more stable 2D HOF networks can be constructed through "shape matching" intermolecular $\pi \cdots \pi$ stacking to establish permanent porosity.⁵³ Porphyrins are attractive candidates for the construction of stable HOFs as their large aromatic tectons can engage in cooperative $\pi \cdots \pi$ stacking between layers, assisting in the construction of robust frameworks. This organization allows for eclipsed stacking that avoids interpenetration through staggered stacking and expands the pore sizes of HOF materials. Chen et al. utilized this strategy by functionalizing 5,10,15,20-tetrakis(4-(2,4diaminotriazinyl)phenyl)-porphyrinato zinc (ZnTDPP) with the hydrogen-bonding 2,4-diaminotriazinyl (DAT) motif, to assemble HOF-7 through 2D layered subunits of ZnTDPP connected by intramolecular hydrogen bonding and $\pi \cdots \pi$ stacking interactions.⁵⁴ Each DAT moiety engages in two types of hydrogen bonding interactions: (i) type I head-to-head N-H...N configurations and (ii) type II head-to-waist N-H...N configurations to self-assemble into 2D layers that interact to form double layers that pack into a 3D framework via $\pi \cdots \pi$ interactions of the ZnTDDP molecules. Due to this framework containing smaller cavities than HOF-11, ranging from 3.2 × 4.7 Å^2 to $4.2 \times 6.7 \text{ Å}^2$, the desolvated HOF-7a allows kinetic cooperativity in selective CO₂/N₂ separations due to the size of the pores matching the size of CO₂. Under similar conditions as those used to study HOF-11, HOF-7 showed a 3-fold higher selectivity for CO₂ in a 15:85 CO₂/N₂ mixture at 273 K and 1 bar. The fitted enthalpy for HOF-7a at zero coverage was calculated to be 32.0 kJ mol⁻¹ for CO₂.

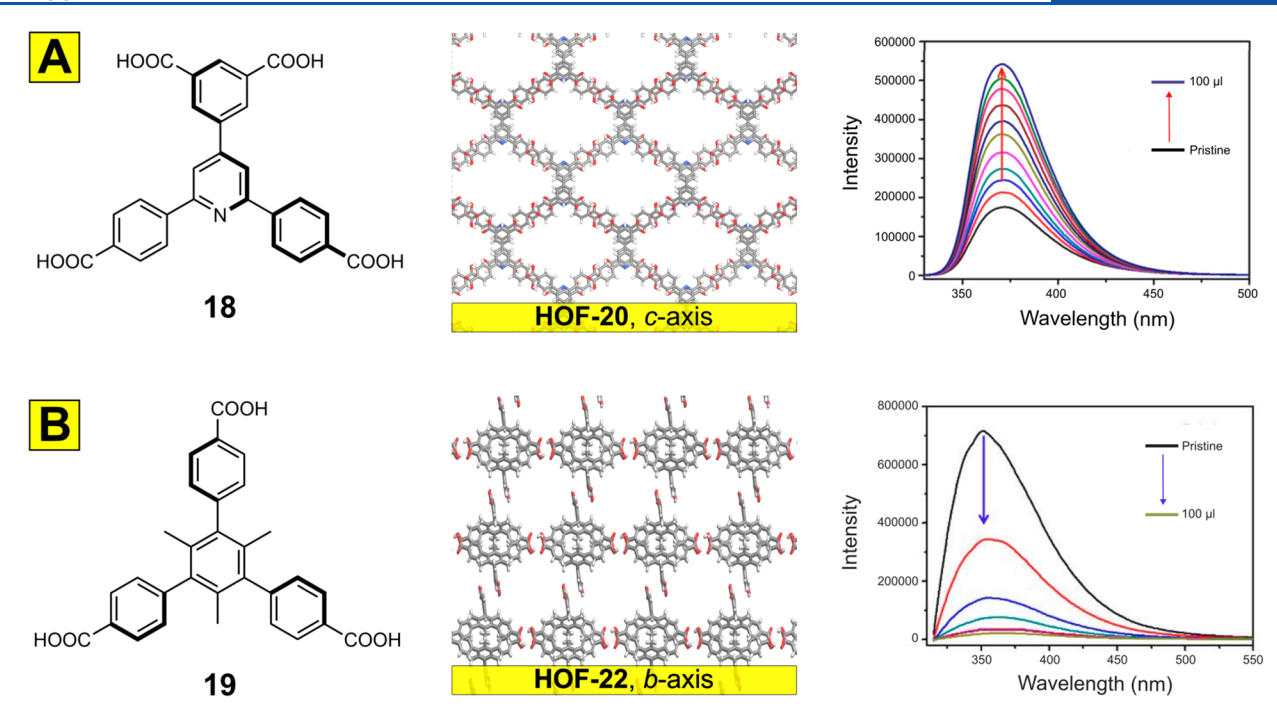
3. MOLECULAR SIEVING

Solution processability of PMCs sets them apart from those of MOFs, covalent organic frameworks (COFs), and zeolites. Cooper et al. have extensively utilized this feature of PMCs to deposit coatings of their imine cages onto thin film composites for selective molecular sieving, so and as chromatography capillary columns for the separation of racemic alcohols and amines. Though these initial studies proved the concept of the utilization of 1b-R in gas chromatography, the system showed a narrow range of enantioselectivities and poor separation, evidenced by broad chromatographic peaks.

The enantioselectivity in the resolution by **1b-R** was increased by Yuan and co-workers by employing polysiloxane (OV-1701) as an additive in the gas chromatography (GC) column preparation. The improved **1b-R** coated column possessed better enantioselectivity and chiral resolution of linear alkanes, alcohols, and aromatic hydrocarbons than the commercially available Chirasil-L-Val and B-DEX 120 columns. The **1b-R** capillary column (column A) was prepared by coating a pretreated fused silica capillary column with a 1.5 mg mL⁻¹ solution of the porous organic cage in dichloromethane at 36 °C, with one end of the capillary maintained sealed and the other connected to a vacuum to slowly evaporate the solvent. The two-component capillary column (column B) was prepared in a similar fashion, but **1b-R** (3 mg mL⁻¹) were

diluted with OV-1701 (4.5 mg mL⁻¹) in an equimolar solution with CH2Cl2. Scanning-electron microscopy (SEM) images of cross-sections from both columns showed a better dispersion and thicker coating on the inner wall of column B than that observed in column A. Due to the better coating of column B, it demonstrated a higher efficiency of 3160 theoretical plates m⁻¹ compared to the 1920 theoretical plates m⁻¹ measured for column A using *n*-dodecane at 140 °C as the reference system. Linear alkanes, alcohols, and aromatic hydrocarbons were tested as solutes for initial investigations of column A. All of the components of the normal alkane mixture $(n-C_6 \text{ to } n-C_2)$ and the aromatic hydrocarbon mixture (benzene, toluene, ethylbenzene, *n*-propylbenzene, *n*-butylbenzene) were baseline resolved and eluted in order of their boiling points. High resolution and sharp peaks were also achieved for the mixture of alcohols (n-C₁ to n-C₈) due to moderate hydrogen bonding interactions of the analytes with the host, 1b-R. Column A also offered good separation of positional halohydrocarbons with elution sequence following the order of ortho-isomer < paraisomer < meta-isomer, which is not the same as what is observed in ordinary capillary columns which typically follow the order of boiling points (meta < para < ortho). The long retention times of meta-substituted compounds can be attributed to the subunit of 1b-R which creates a 3-fold symmetry axis, kinetically favoring the meta-substitution geometries. Similarly, column B demonstrated excellent enantioselectivity for the separation of a wide range of racemates, apart from chiral alkanes, which are too large to pass between the 0.58–0.76 nm cavities of the POCs. Though it is difficult to fully understand the overall influences of the chiral microenvironment of crystalline 1b-R on these chromatographic separations, the authors were able to deduce that a multimodal enantioselective retention mechanism exists in the system as a one component chiral recognition mechanism would not be able to effectively resolve alcohols, diols, amines, alcohol amines, esters, ketones, ethers, halohydrocarbons, organic acids, amino acid methyl esters, and sulfoxides. Furthermore, column B showed high thermal stability (up to 260 °C) and separation repeatability reinforcing its practical use. These results demonstrate 1b-R as a very attractive stationary phase in GC outcompeting highly selective reference capillary columns currently on the market.

Though our understanding of PMCs in chromatographic separations is still in its infancy, Chen and co-workers have also demonstrated that HOFs can be used in enantioselective separations of small alcohols at room temperature.⁵⁸ They functionalized the chiral building block 1,1'-bi-2-naphthol-(BINOL) with the popular DAT moiety to successfully produce the homochiral HOF-2. This framework has a unimodal 6-connected {3355667} 3D networking with 1D hexagonal pores 4.8 Å in diameter. The activated HOF-2 has a BET surface area of 237.6 $\mathrm{m}^2~\mathrm{g}^{-1}$, based on its CO_2 adsorption isotherm and exhibits high chiral separation of secondary aromatic alcohols. The chiral cavities of the framework show particularly high recognition of (R)-1-phenylethanol (R-1-PEA) achieving enantioselective separation up to 92% ee. This observation can be explained by the preferred confinement of R-1-PEA in the chiral pockets of the framework along with strong hydrogen-bonding interactions between the -OH groups of the analyte and the oxygen atoms from the diethoxy moieties of the HOF-2 framework. It can also achieve separation of 2-butanol (77% ee) and 2-pentanol (48% ee), as well as other secondary alcohols of pharmaceutical interest:



www.acsanm.org

Figure 8. (A) Turn up fluorescence exhibited by HOF-20 in the presence of aniline. (B) Turn down fluorescence exhibited by HOF-22 was turned down in the presence of nitrasone. Solvent was emitted for clarity. Element colors: C—gray, H—white, O—red.

1-(4-chlorophenyl)ethanol (79% ee) and 1-(3-chlorophenyl)ethanol (66% ee).

4. ANALYTICAL APPLICATIONS

4.1. Fluorescent Sensing. Molecular recognition plays an important role in biological and chemical systems, typically through specific complementary interactions between two or more molecules. Utilization of weakly bonded PMCs in specific and selective recognition necessitates they be permanently porous and stable in aqueous media for environmental relevancy. In the case of fluorescent sensing, the analyte also needs to strongly interact with the host to alter its fluorescent properties. These changes in fluorescence can be detected by either turn-down or turn-up responses, with the latter being more desirable but harder to achieve.

Only a handful of HOFs have shown good stability in water, with aromatic-rich linkers decorated with carboxylic acid moieties seemingly being the most promising platforms for this high aqueous resistance. Chen and co-workers have reported three systems self-assembled from carboxylate dimer interactions for molecular sensing in aqueous media: HOF-20,59 HOF-22,60 and HOF-FAFU-1.61 The first of these is a 3D HOF constructed from 5-(2,6-bis(4-carboxy phenyl)pyridin-4yl)isophthalic acid (18). HOF-20 features 1D channels of 13 in diameter created through hydrogen bonding of the carboxylic acid termini and $\pi \cdots \pi$ stacking of the aromatic skeleton of this tetratopic organic linker (Figure 8A left and center). The activated HOF-20 has a BET surface area of 1323 m² g⁻¹ and is stable in water, even at elevated temperatures and in the presence of acid. Upon exposure to aniline, the fluorescence of HOF-20 is enhanced (Figure 8A right) with a detection limit toward the analyte of 2.2 µM and efficiency of 142%, even in the presence of other aromatic molecules. In this HOF, aniline is forming intermolecular interactions with the framework that restrict the twisting rotations of the aromatic rings in the skeleton of the linker, reducing the nonradiative

decay pathways after photoexcitation. The framework can be easily regenerated through aqueous washing and shows good recyclability with minor loses in its aniline sensing efficiency. Similar aromatic-rich tetratopic carboxylic acid organic linkers were used in the construction of PFC-1⁶² and HOF-14;⁶³ these materials engaged in weaker interactions with aniline, with lower fluorescence enhancement efficiencies of 7% and 18%, respectively.

More common turn-down fluorescent responses, such as that shown on the right of Figure 8B, were observed in HOF-2260 and HOF-FAFU-1.61 The former showed fluorescent quenching in the presence of organoarsenics, while the latter was used for sensing of hypochlorite. Both analytes are of interest to human health, as organoarsenic compounds are used as livestock feed additives and hypochlorite is found in household bleach and disinfectants, which pollute drinking water. HOF-22 was constructed using a tricarboxylic acid organic building unit, 5'-(4-carboxyphenyl)-2',4',6'-trimethyl-[1,1'-3',1'-terphenyl]-4,4''-dicarboxylic acid (19), to produce a 2-fold interpenetrated 3D HOF (Figure 8B left and center). Two organic arsenics were selected for the sensing studies, roxarsone (ROX) and nitarsone (NIT), due to their importance in the livestock industry. The quenching efficiencies of these systems were found to be 93% for ROX and 97% for NIT. It is hypothesized that the primary quenching mechanism for NIT is a photoinduced electron transfer (PET) process, but an observed blue-shift in the emission spectra after the addition of ROX pointed toward a combined Förster resonance energy transfer (FRET) and PET process in the detection of this analyte. Furthermore, the methyl groups in the central benzene of the OBU in HOF-22 assisted in restricting rotation of the arm moieties around the carbon-carbon bond connecting them to the central ring, efficiently reducing the nonradiative pathways.

Recently, Chen and co-workers reported a new strategy to produce permanently porous HOFs with increased stability in

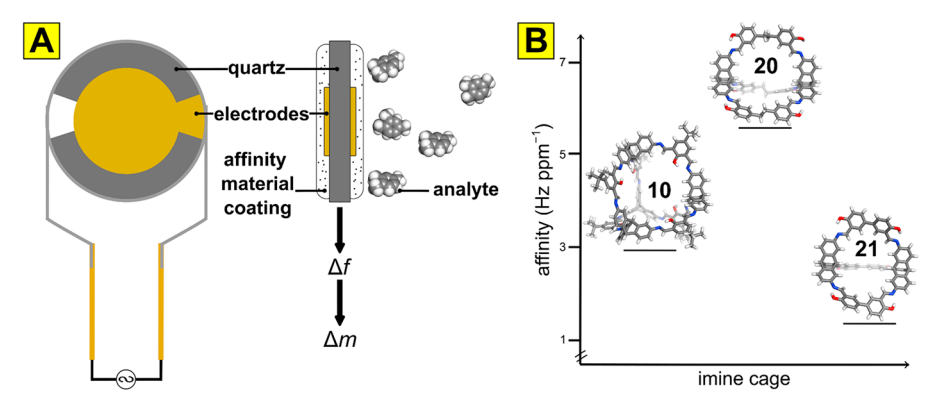


Figure 9. (A) Schematic arrangement of the components in a simple QCM with pseudocumene molecules shown as the analyte, and the responses gathered from the device. (B) Comparison of the affinity of three different imine cages, 14, 20, and 21 for pseudocumene. Element colors: C—gray, H—white, N—blue, O—red.

aqueous media by utilizing free hydroxyl or amino moieties within structures to enlarge the π -conjugated systems. Framework HOF-FAFU-1⁶¹ was a modified version of HOF-TCBP decorated with free hydroxyl groups. HOF-TCBP selfassembles from 3,3',5,5'-tetrakis(4-carboxyphenyl)-1,1'-biphenyl (H₄TCBP) into a distorted tetrahedral configuration; however, the addition of -OH moieties in HOF-FAFU-1 prevents puckering of the inner biphenyl C-C bond and planarizes the structure. Flattening the scaffold by employing 3,3',5,5'-tetrakis(4-carboxyphenyl)-4,4'-dihydroxy-1,1'-biphenyl (4,4'-OH-TCBP) allowed the authors to incorporate a combination of $\pi \cdots \pi$ stacking between the aromatic skeleton and hydrogen-bonding via carboxylic acid dimers to construct a robust 3D porous framework. Each 4,4'-OH-TCBP unit is connected to four neighboring buildings blocks engaging in four pairs of carboxylate dimers to form a 2D layer which interacts with two adjacent layers through stabilizing face-toface $\pi \cdots \pi$ stacking interactions. This produces a nanoscale structure with rhombic channels containing apertures up to 28.1 in size and a BET surface area of 840 m² g⁻¹. Upon exposure to hypochlorite, this material exhibits a fast turndown fluorescent response reaching equilibrium within 15 s and with a detection limit of 1.32 μ M. This response is beneficial for real-time sensing and can be attributed to the mesopores of HOF-FAFU-1 which facilitate the mass transfer of hypochlorite within the channels. No fluorescent response was observed by HOF-TCBP, suggesting a critical role of the hydroxyl moieties. The sensing specificity and selectivity for hypochlorite was tested against more than a dozen common coexisting ions, and no competition was observed. The authors determined a static quenching mechanism was responsible for the fluorescent quenching of the system which they attributed to a transformation from a fluorescent species to a nonfluorescent one. This hypothesis was further strengthened by UV/vis spectroscopy experiments in which they observed a blue-shift of the adsorption band of 4,4'-OH-TCBP pointing toward the formation of a nonfluorescent oxidative state upon exposure to hypochlorite as the oxidant.

Substituted pillar[5] arenes have been used as nanoporous platforms for the fluorescent detection on n-alkanes. 62

4.2. Sensing Devices: Quartz Crystal Microbalances. Quartz crystal microbalances (QCMs) are low-cost mobile technologies suitable for the construction of continuously working sensors. A typical QCMs is composed of a piezoelectric quartz crystal sandwiched between two electrodes. An affinity material is then coated over the electrodes, and

the binding of analytes onto it creates a shift on the oscillation frequency of the device which can be detected (Figure 9A). Selective detectors can be designed by coating a QCM with compounds whose functional groups are capable of binding analytes with high specificity. These binding sites must be easily accessible to achieve a fast response and be able to reversibly adsorb/desorb the guest molecules for quick regeneration of the sensors. In 2012, Mastalerz and Waldvogel demonstrated that PMCs can be processed into thin film coatings to build operationally simple QMCs. The PMCs were synthesized through the imine condensation of 15 with either 2-methoxyisophthalaldehydes (such as 16 for the synthesis of 14) to produce the end-functionalized [4 + 6] cage compounds or bis(2-hydroxybenzaldehydes) to produce the exofunctionalized [2 + 3] cages 20 and 21.

These affinity materials were then deposited onto QCMs with a 195 MHz fundamental frequency to produce a device for the sensing of aromatic vapors present in rodenticides. The more flexible [2 + 3] POC 20 constructed using 5,5'-(ethane-1,2-diyl)bis(2-hydroxybenzaldehyde) showed superior sensitivity for p-xylene and m-xylene than the perallylated β - and γ -cyclodextrins, ⁶⁶ the best performing affinity materials at the time, and the highest affinity for pseudocumene among POCs (Figure 9B). This study further demonstrated the ease with which functional groups can be incorporated into POCs to achieve selective binding of analytes, a feature that is synthetically challenging in cyclodextrins. This example critically exploited the processability of PMCs for the purpose of developing novel technologies for analyte detection.

The detection of narcotics and illegal drugs is another societal issue that requires efficient and portable sensing devices. On-site detection of hazardous and controlled substances such as amphetamines, γ -hydroxybutyric acid (GHB) and their precursors safrole, (—)-norephedrine, phenylacetone, and γ -butyrolactone (GBL) is commonly conducted through ion mobility spectrometry. However, QCMs have gained popularity as a cheaper alternative for portable and sensitive illicit drug sensing. Initial studies focused on the detection of GBL by tailor-made adamantoid [4 + 6] imine POC 14. 19 The high affinity for GBL is achieved through strong hydrogen bonding with the ammonium moieties of the intramolecularly protonated cage. However, the hydrolytic sensitivity of the imine bonds connecting the cages has limited its applications.

To combat the issues of bond dissociation, the next generation of QCMs utilized organic molecules of intrinsic microporosity (OMIMs). OMIMs are a class of porous organic materials constructed from discrete oddly shaped concave OBUs that achieve porosity by maximizing free volume through their inefficient packing. This "packing frustration" gives them the advantage of maintaining microporosity, even in the amorphous state. In 2019, Mastalerz et al. reported five OMIM building blocks (22–26) synthesized from a triptycene core with a 3-fold symmetry (15) and π -planes of varying lengths. OMIM 22 is the smallest derivative (Figure 10A),

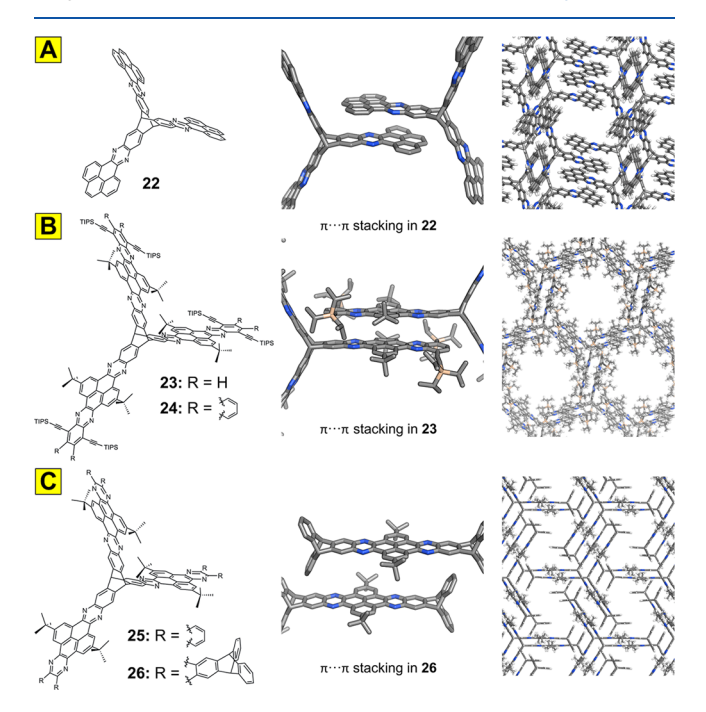


Figure 10. Triptycene based OMIMs 22-26 engage in varying degrees of π ··· π stacking due to the steric effects of their substituents. (A) OMIM 22 contains the shortest aromatic π -planes and forms 1D ribbons in its extended structure. (B) The bulky TIPS substituents in OMIM 23 assist in creating the most porous framework in the series, forming a honeycomb-like architecture, while (C) the OMIM with the longest aromatic π -planes (26) forms aggregates. Hydrogens in the middle row structures were omitted for clarity. Element colors: C—gray, H—white, N—blue, O—red, Si—blush.

while OMIM 26 contains the longest aromatic π -plane (Figure 10C). These affinity materials combine rigid organic backbones with well-defined intermolecular free volumes to create frameworks with high specific surface areas of up to 754 m² g^{-1} . The $\pi \cdots \pi$ stacking features in each framework differ due to the steric effects of the substituents, and this in turn also affects their packing architectures, with OMIMs 23 and 24 creating honeycomb-like structural arrangements, one of which is shown on the right of Figure 10B, OMIM 22 forming onedimensional ribbons (Figure 10A, right), and OMIM 26 aggregated layers (Figure 10C, right). The affinity materials deposited onto the QMC were tested against the narcotic precursors. The authors determined that safrole, piperonal, and phenylacetone engaged in $\pi \cdots \pi$ interactions with the electron deficient π -units of the OMIMS while the nonaromatic piperazine, piperidine, cyclohexanone, and GBL interacted via hydrogen bonding and van der Waals interactions. OMIM 24 exhibited the highest affinity for all analytes, and this could be attributed to the elongated π -system of this compounds which forms larger voids and the sterically demanding TIPS-

ethynyl substituents which induce more accessible binding sites. This affinity material had the highest selectivity to safrole, a precursor to ecstasy, reaching a 30% higher Δf for this analyte than any other and is capable of detecting it at concentrations down to 0.11 ppb. The drawback of these systems is that they undergo nonspecific adsorption; therefore, they cannot be used for multisensing purposes, but they can be implemented into a sensor array. This study demonstrates the importance of sterics and π -conjugation in synthesizing efficient affinity materials. The systematic investigation of resorcin[4]arene-based cavitands by Waldvogel and co-workers established an expected correlation between the cavity shape and size of PMCs and affinities for specific guests. The systematic investigation of the systematic investigation of resorcin [4] arene-based cavitands by Waldvogel and co-workers established an expected correlation between the cavity shape and size of PMCs and affinities for specific guests.

5. NEW FRONTIERS IN THE APPLICATIONS OF PMCS

5.1. Proton Conduction. Fuel cells can be divided into five categories because of their electrolyte: proton exchange membrane fuel cells (PEMFCs), alkaline fuel cells (AFCs), solid oxide fuel cells (SOFCs), molten carbonate fuel cells (MCFCs), and phosphoric acid fuel cells (PAFCs). PEMFCs are the most efficient due to their short startup times, low reaction temperatures, high energy density, and long lifetimes. The proton exchange membrane (PEM) is a critical component of the system, as it dictates the lifespan of the cell. While MOFs have been tested for MEA applications, their limitations in aqueous media make most of these materials unsuitable for the moisture levels in fuel cells. This, along with their inherent flexibility and solution processability, makes PMCs better suited for membrane fabrication to produce lightweight conducting electrodes.

Several HOFs have been shown to facilitate proton conduction in fuel cells. Most of the studied systems have been constructed from ionic backbones, namely, arene sulfonates and guanidinium-ion OBUs. Ghosh et al. reported two HOFs, HOF-GS-10 constructed from 1,5-napthalenedisulfonic acid and guanidine hydrochloride and HOF-GS-11 constructed from 4,4'-biphenyldisulfonic acid and guanidine hydrochloride.⁷⁴ The disulfonate units in HOF-GS-10 interact with six guanidinium motifs to form quasi-hexagonal sheets that pack in stacks of two with naphthalene acting as a pillar separating one sheet from another, forming 2D structures with 1D square-like channels. A similar bilayer structure is present in HOF-GS-11 via ribbon hydrogen-bonded sheets formed by each disulfonate unit interacting with eight guanidinium motifs. These layers arrange with biphenyl pillars separating them to create 1D rectangular-like channels. Both HOFs are stable to moisture and can be activated to produce permanent porous frameworks. Water sorption studies revealed that HOF-GS-11 has a 3.3-fold higher water uptake than HOF-GS-10 (11.6 mmol g^{-1} vs 3.47 mmol g^{-1}), and—due to water molecules serving as the proton carriers in these systems—this difference translates into higher proton conductivity for HOF-GS-11. At 95% relative humidity, HOF-GS-11 has a proton conductivity of 1.8×10^{-2} S cm⁻¹ while HOF-GS-10 has a proton conductivity of 0.75×10^{-2} S cm⁻¹. Low activation energy of HOF-GS-11 rivals that of HPF2-100, the lowest activation energy reported in literature.⁷⁵ The low activation energies for both frameworks (below the 0.4 eV threshold) correspond to a Grotthus-type mechanism where a hydronium ion reorients and passes its proton to a neighboring molecule through a hydrogen bond facilitated proton transport. The differences in their values are explained by the more hydrophobic nature of HOF-GS-10 arising from the

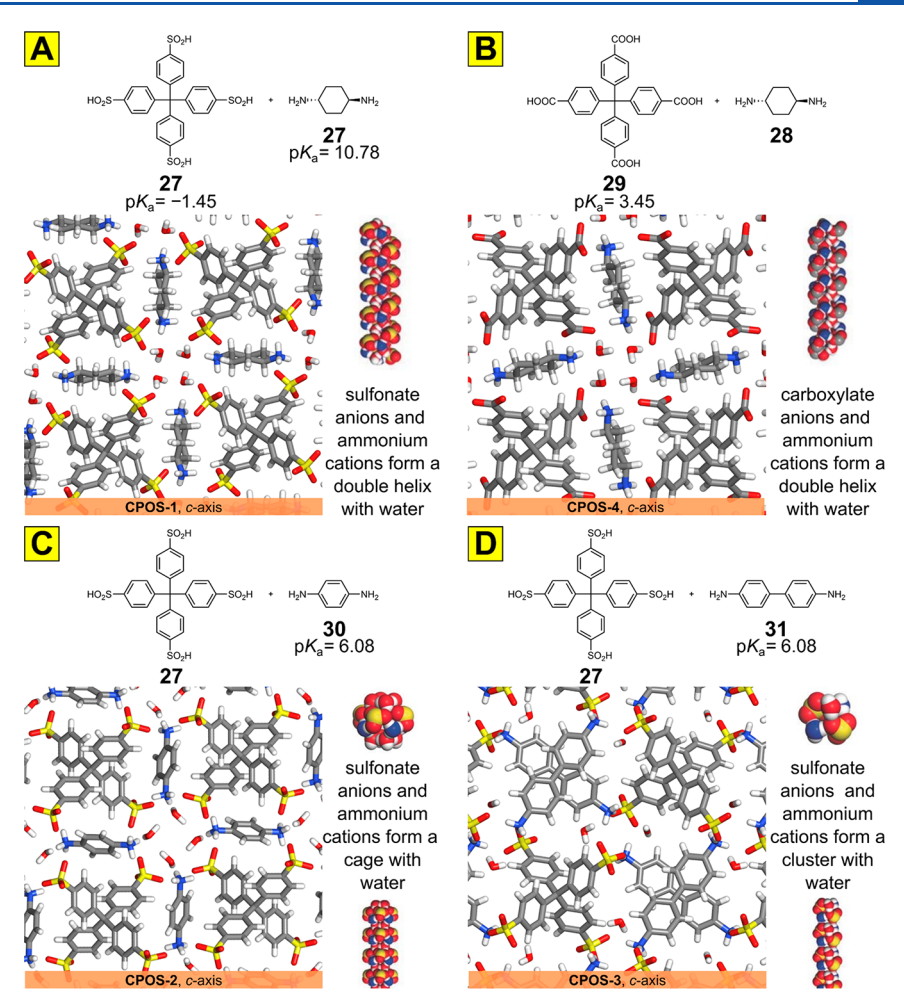


Figure 11. Ionic building units and crystal structures for porous organic salts CPOS-1, 2, 3, and 4. (A) The 1D channels of CPOS-1 create a double-helix structure with water between the sulfonate anions and ammonium cations. (B) A double-helix structure similar to that with water is observed in the 1D channels of CPOS-4 with the carboxylate anions and ammonium cations. (C) Water molecules within the 1D cages of CPOS-2 arrange themselves around the sulfonate and ammonium ions to form cage structures, while in (D) in the 1D channels of CPOS-3 they form cluster structures. Element colors: C—gray, H—white, N—blue, O—red, S—yellow. Adapted with permission from ref 76. Copyright 2018, Wiley.

naphthalene motifs. This work highlights the promise of porous structures held together by weak interactions as solid-state materials for fuel cells.

Similar proportional behavior of proton conductivity to water content was observed by Ben et al. in their crystalline porous organic salt (CPOS) systems.⁷⁵ Though in the case of HOF-GS-10/11, water content within the channels was a factor of hydrophobicity, CPOSs' water uptakes are a factor of binding affinities within their pores. CPOSs are noncovalently connected frameworks self-assembled via ionic acid-base interactions that give rise to 3D networks containing 1D polar channels. The authors produced four different derivatives through different acid-based combinations: tetrakis(4sulfophenyl)methane (27) paired with either trans-1,4diaminocyclohexane (28), p-phenylenediamine (30), or benzidine (31) and tetrakis(4-carboxyphenyl)methane (29) paired with 28. They can all be activated, and the desolvated CPOSs have surfaces between 12 and 216 m² g⁻¹. Despite having a moderately high surface area, CPOS-4 exhibits low stability due to its weak ionic bonds. Varying degrees of hydrogen-bonded chains through charge-assisted N-H···O interactions within the frameworks as well as the water guests residing within the pores help facilitate the proton transport and conductivity in CPOS-1, CPOS-2, and CPOS-3 (Figures

11A, C, and D). At 98% relative humidity and 333 K, the proton conductivities of CPOS-1 through CPOS-3 are 1.0×10^{-2} S cm⁻¹, 2.2×10^{-2} S cm⁻¹, and 3.7×10^{-4} S cm⁻¹, respectively. Along with having the highest proton conductivity among all derivatives, CPOS-2 also had the highest measured water content of 10.67% which accounts for 5 molecules of water per salt. Furthermore, their activation barriers—ranging from 0.61 to 0.93 eV—reveal a vehicular mechanism responsible for proton transport within these noncovalent organic frameworks.

One limitation of proton conduction in PMCs has been the tendency for directional proton transport in a 1D space on account of the low-dimensional pore structures in most of the frameworks tested, including the two systems mentioned above. In this context, 3D mobility could be enhanced by introducing defects in structures, decreasing the overall crystallinity of frameworks, or—as was shown by Cooper et al. The predesigning porous molecular solids that can be directed to adopt 3D pore topologies by virtue of their native structures and therefore enhance mass transport properties. The authors tested two nitrogen-containing porous organic cages, 1b (imine cage) and 4a (the reduced amine cage of 1a). The neutral imine cage, 1b, was able to reversibly absorb up to 20.1 wt % water, which equates to 12 molecules of H₂O per

Figure 12. Transformations of imine cages 1a and 1b to reduced secondary amines 4a and 4b (middle), respectively. Secondary amine cage 4a can then be protonated to form cages 32 and 33 (right).

cage and reaches proton conductivities of up to 6.4×10^{-6} S cm⁻¹ at 95% RH and 303 K, similar to what has been reported by neutral intrinsically porous cucurbit [6] uril. ⁷⁸

Cage 4a was transformed into two different crystalline salts, cage 32 with a chemical formula $(H_{12}RCC1)^{12+} \cdot 12Cl^- \cdot 4(H_2O)$ and cage 33 with a chemical formula $(H_{12}RCC1)^{12+} \cdot 6(SO_4)^{2-}$ 27.25(H₂O), to improve its activity and test the effect of ion size on proton conductivity (Figure 12). Due to the direct correlation between water uptake and proton mobility exhibited by these three cages, at low humidity levels of 30% RH, the chlorinated and sulfonated salts had low proton conductivities of $1.0 \times 10^{-4} \text{ S cm}^{-1}$ and $3.2 \times 10^{-8} \text{ S cm}^{-1}$ respectively. The proton conductivity of 33 is >3000-times lower than that of 32 under the same conditions, on account of water molecules initially arranging themselves around the anionic SO_4^{2-} units eventually restricting the diffusion of H_2O into the cage cavities. However, as the relative humidity is increased to 95% RH, the proton conductivity increases to 6.1 \times 10⁻⁵ S cm⁻¹, which is 20-fold lower than the proton conductivity of the chlorinated salt $(1.1 \times 10^{-3} \text{ S cm}^{-1})$. Though the overall proton conductivities of 33 are lower than those of 32, the former system experiences a 2,000-fold faster increase in proton conductivity going from 30% to 95% RH, suggesting that the water content within its cavities dramatically increases as a factor of humidity. In the case of 32, the high proton conductivities, approaching the highest reported for MOFs, 79 can be attributed to the slow translational diffusion of H₂O molecules occupying the cavities of the salt leading to increased water retention and therefore enhanced water-mediated proton conductivity. Water mobility also plays a role in the activation energies of these materials. The Arrhenius plots at 95–98% RH yielded activation energies of 0.11 0.35, and 0.10 eV for 1b, 32, and 33, respectively, all pointing toward a Grotthuss mechanism like that of HOF-GS-11. The differences in the activations energies for both salts can be explained by the water diffusion dynamics in each system: in both structures, it is energetically favorable for a water molecule in the intrinsic cavity to move toward the cage windows where the anions reside. However, it is significantly more difficult for the molecule in 33 to transverse the window due to the larger size of the SO_4^{2-} divalent anions, therefore needing a higher activation energy to exit.

5.2. Porous Liquids. On an intuitive level, porosity is a property inherently associated only with the solid state, in which the relative immobility of molecules allows the

formation of noncollapsible empty voids. The concept of liquids retaining permanent porosity has gained a lot of attention since it was first proposed by James and co-workers in 2007. They also divided porous liquids into three groups: Type I is a neat liquid of fluid hosts, and Types II and III are composed of a host with empty cavities dissolved or suspended, respectively, in a sterically hindered solvent.

In a seminal 2015 paper, 81 Copper, James, and co-workers reported the first example of a Type II porous liquid. They showed that if the components of a PMC are dissolved in a solvent whose molecules are too large to enter the internal cavity, then porosity persists even in solution. The authors achieved this by synthesizing a POC through the imine condensation of 2 and crown-ether diamine with overall yields of 3.1-6.5%. The cages have an inner diameter of 5 with the accessible windows measuring 4 Å. The bulky crown ether was used as the solvent for these cages: using 15-crown-5 (15-C-5), a 44 wt % solution could be prepared, and it remained fluid at room temperature. The empty voids were confirmed through molecular dynamics and positron (e^+) annihilation lifetime spectroscopy. Upon introducing methane into the porous liquid, the solubility of this gas in 15-C-5 increased 8-fold (6.7 μ mol g⁻¹ in the neat 15-C-5 solution vs 52 μ mol g⁻¹ in the imine cage porous liquid), therefore proving the cages can accommodate guests in solution. However, the high content of bulky crown ether solvents limited the accessible pore volume of the POC, and the overall low yield prevented practical scale-

Cooper and co-workers next designed a strategy to prepare scalable porous liquids by synthesizing "scrambled cages". 82 They prepared a racemic mixture of imine cages from 2, R,R-3c, and 3a in a 4:3:3 ratio. The structural disorder and inability to easily pack in the solid state gave this material an inherently higher solubility in organic solvents in comparison to enantiopure analogues,83 and a porous liquid could be prepared by dissolving these cages in hexachloropropene (PCP) with high solubility up to 242 mg mL⁻¹. The resulting solution was ten-times less viscous than the 15-crown-5 liquid and had comparable methane solubility of 51 mg mL⁻¹. Due to the size and shape of the cavity better accommodating chloroform in the voids, the addition of this solvent into the porous liquid expelled the methane molecules from the host cages—this was observed by the evolution of gas upon the addition of chloroform. Various other guests such as Xe, SF₆, and CO₂ were adsorbed by this porous liquid with their

solubility increasing by up to 20% in comparison to neat PCP. 84 However, the high volatility of PCP prevents this porous liquid from being used in high pressure or high temperature settings. Further studies from Cooper and coworkers focused on automating the synthesis of these scrambled cages through high-throughput robotic workflow ultimately leading to a library of 44 different racemic cage mixtures prepared from the imine condensation of 2 and 11 readily available amines.⁸⁵ The solubility of all 44 cage mixtures was tested, and 40 of them were found to have solubilities higher than 300 mg mL⁻¹ in five bulky aromatic solvents (2,4-dichlorobenzyl chloride, 2,4-dichlorotoluene, 4trifluoromethoxybenzyl alcohol, o-hydroxyacetophenone, and methyl salicylate) while 27 had comparable solubility in PCP (>200 mg mL⁻¹) to the original scrambled cage mixture. While these approaches opened the interest in porous liquids, they clearly remained niche as they required exotic solvents larger than the cavity of intrinsic PMCs dissolved in it.

To combat problems of solvent selection and limited pore volumes associated with Type II porous liquids, Dai and coworkers reported a porous ionic liquid prepared through the supramolecular complexation of an anionic porous organic cage and a counterion too large to enter the cage cavity. 86 This allowed for the direct liquefaction of the POC as ionic liquids typically have low melting points. The POC was synthesized by the imine condensation of 2 with 3a and $6^-\cdot K^+$ to produce a modified version of Cooper's imine cage 1a¹⁶ with an anionic carboxylate group and potassium (K+) counterion (dubbed KACC). The substitution of one of the ethylenediamine subunits with the ionic moiety led to a loss of symmetry and thus crystallinity. The Type I porous liquid was then prepared by physically mixing KACC with dicyclohexano-18-crown-6 (18-C-6) to afford 18-C-6/K+ supramolecular complexes as the counterion and thus a viscous porous ionic liquid (18-C-6-PL) with a glass transition point of -30 °C and melting point of 50 °C. A similar approach was attempted by using 15-C-5, but this led to a Type II porous liquid due to the cage complexes dissolving in excess 15-C-5. The permanent porosity of both systems was confirmed by molecular dynamics and PALS, and the supramolecular complexation between the crown ethers and potassium salts was confirmed through thermogravimetric analysis (TGA) which showed a stronger interaction of K⁺ with 18-C-8 than 15-C-5 pointing toward a lower volatility of the former porous ionic liquid. The cavity diameters for 18-C-6-PL and 15-C-5-PL were calculated to be 4.6 and 4.4, respectively, which are large enough to accommodate small gases such as CO₂ and N₂. The enhanced gas sorption capacity of 18-C-6-PL was confirmed through CO2 adsorption/ desorption isotherms, which revealed 18-C-6-PL had a CO₂ sorption capacity of 0.429 mmol g⁻¹, while 18-C-6 showed virtually no gas uptake. This approach was a lot more successful than a previous attempt by James and co-workers to make Type I porous liquids by modifying CC1 imine cages with alkyl chains to limit their packing ability and lower their melting point as low as 50 °C. 87 Unfortunately the alkyl chains interpenetrated the cavities of neighboring cages decreasing the pore volumes by 90-100%.

Porous liquids have the potential to revolutionize the field of microporous fluids and functional hierarchical materials. Although most porous liquids have been used for gas capture, some have been explored for catalysis, ⁸⁸ and chiral separations. ⁸⁹ There are still a variety of challenges associated with porous liquids, including their viscosity, preparation, high

melting points, and stability, but recent advances in their design based on covalently stabilized nanocomposites and ionic-liquid-based solutions and colloidal suspensions present opportunities for emerging properties more attractive than those of traditional solid-state PMCs or polymeric networks.

6. OUTLOOK AND PERSPECTIVE

Chemistry of PMCs is blossoming, and their first applications are emerging in a variety of areas. Some of them-in gas storage and separations—are closely related to the similar uses of other classes of porous materials, particularly, MOFs and COFs. PMCs' benefits in these comparisons come from their highly modular pore structures, which can be synthetically finely tuned to match the sizes of particular guests-thus enabling highly selective separations of closely related species. In other applications, such as molecular sensing or the preparation of porous liquids, the solubility and solutionphase processability allow uses in contexts that are either completely unavailable to other classes of porous materials or significantly more difficult to achieve. Important challenges still remain, however. Preparing PMCs at scale is often difficult: many are based on hydrolytically or chemically labile functional groups. PMCs that are extrinsically porous are often polymorphous with the porous phase being a kinetic product.

In our view, future efforts on the development of PMCs should focus on addressing ways to (a) introduce strong guest binding sites into pores of these frameworks, either through presynthetic design or postsynthetic modification, (b) engineering of stabilizing interactions to assist in retaining their permanent porosity, (c) preparing composite materials with PMCs as active components, and (d) establishing a clearer relationship between the molecular properties of PMC building blocks and the behavior of the crystal as a whole. This last point is particularly salient as porous liquids now bridge the divide between individual molecules and virtually perfectly ordered crystals. Such an understanding could also help in the utilization of amorphous porous molecular materials, which are at present probably often overlooked in favor of their crystalline counterparts.

AUTHOR INFORMATION

Corresponding Author

Ognjen S. Miljanić — Department of Chemistry, University of Houston, Houston, Texas 77204-5003, United States;
orcid.org/0000-0002-7876-9034; Email: miljanic@uh.edu

Author

Alexandra Robles – Department of Chemistry, University of Houston, Houston, Texas 77204-5003, United States

Complete contact information is available at: https://pubs.acs.org/10.1021/acsanm.3c02188

Author Contributions

The manuscript was written through equal contributions from both authors. Both authors have given approval to the final version of the manuscript.

Notes

The authors declare no competing financial interest.

ACKNOWLEDGMENTS

Work in our group over the years was generously supported by the University of Houston, the National Science Foundation (awards DMR-1507664, DMR-1904998, and CHE-2204236 to O.Š.M.), the Welch Foundation (award E-1768 to O.Š.M.), and the donors of the American Chemical Society Petroleum Research Fund (award 58919-ND4 to O.Š.M.). O.Š.M. gratefully acknowledges the support from the Alexander von Humboldt Foundation for his sabbatical stay at the Ruprecht-Karls-Universität in Heidelberg (Germany), where parts of this manuscript were written.

REFERENCES

- (1) Wang, X.; Simard, M.; Wuest, J. D. Molecular Tectonics. Three-Dimensional Organic Networks with Zeolitic Properties. *J. Am. Chem. Soc.* **1994**, *116*, 12119–12120.
- (2) Holst, J. R.; Trewin, A.; Cooper, A. I. Porous Organic Molecules. *Nat. Chem.* **2010**, *2*, 915–920.
- (3) Kohl, B.; Rominger, F.; Mastalerz, M. Crystal Structures of a Molecule Designed Not To Pack Tightly. *Chem. Eur. J.* **2015**, *21*, 17308–17313.
- (4) Pulido, A.; Chen, L.; Kaczorowski, T.; Holden, D.; Little, M. A.; Chong, S. Y.; Slater, B. J.; McMahon, D. P.; Bonillo, B.; Stackhouse, C. J.; Stephenson, A.; Kane, C. M.; Clowes, R.; Hasell, T.; Cooper, A. I.; Day, G. M. Functional Materials Discovery Using Energy-Structure-Function Maps. *Nature* **2017**, *543*, 657–664.
- (5) Hashim, M.; Hsu, C.-W.; Le, H.; Miljanić, O. Š. Organic Molecules with Porous Crystal Structures. *Synlett* **2016**, 27, 1907–1918
- (6) Chen, L.; Zhang, B.; Chen, L.; Liu, H.; Hu, Y.; Qiao, S. Hydrogen-bonded Organic Frameworks: Design, Applications, and Prospects. *Mater. Adv.* **2022**, *3*, 3680–3708.
- (7) Little, M. A.; Cooper, A. I. The Chemistry of Porous Organic Molecular Materials. *Adv. Funct. Mater.* **2020**, *30*, 1909842.
- (8) Mastalerz, M. Porous Shape-Persistent Organic Cage Compounds of Different Size, Geometry, and Function. *Acc. Chem. Res.* **2018**, *51*, 2411–2422.
- (9) Evans, J. D.; Sumby, C. J.; Doonan, C. J. Synthesis and Applications of Porous Organic Cages. *Chem. Lett.* **2015**, *44*, 582–588
- (10) Evans, J. D.; Jelfs, K. E.; Day, G. M.; Doonan, C. J. Application of Computational Methods to the Design and Characterisation of Porous Molecular Materials. *Chem. Soc. Rev.* **2017**, *46*, 3286–3301.
- (11) Deegan, M. M.; Dworzak, M. R.; Gosselin, A. J.; Korman, K. J.; Bloch, E. D. Gas Storage in Porous Molecular Materials. *Chem. Eur. J.* **2021**, *27*, 4531–4547.
- (12) Kerry, F. G. Industrial Gas Handbook: Gas Separation and Purification; CRC Press: Boca Raton, FL, 2007.
- (13) Darby, S.; Hill, D.; Auvinen, A.; Barros-Dios, J. M.; Baysson, H.; Bochicchio, F.; Deo, H.; Falk, R.; Forastiere, F.; Hakama, M.; Heid, I.; Kreienbrock, L.; Kreuzer, M.; Lagarde, F.; Mäkeläinen, I.; Muirhead, C.; Oberaigner, W.; Pershagen, G.; Ruano-Ravina, A.; Ruosteenoja, E.; Rosario, A. S.; Tirmarche, M.; Tomáscaronek, L.; Whitley, E.; Wichmann, H.-E.; Doll, R. Radon in Homes and Risk of Lung Cancer: Collaborative Analysis of Individual Data from 13 European Case-Control Studies. *BMJ.* 2005, 330, 223.
- (14) Van Heest, T.; Teich-McGoldrick, S. L.; Greathouse, J. A.; Allendorf, M. D.; Sholl, D. S. Identification of Metal-Organic Framework Materials for Adsorption Separation of Rare Gases: Applicability of Ideal Adsorbed Solution Theory (IAST) and Effects of Inaccessible Framework Regions. J. Phys. Chem. C 2012, 116, 13183–13195.
- (15) Chen, L.; Reiss, P. S.; Chong, S. Y.; Holden, D.; Jelfs, K. E.; Hasell, T.; Little, M. A.; Kewley, A.; Briggs, M. E.; Stephenson, A.; Thomas, K. M.; Armstrong, J. A.; Bell, J.; Busto, J.; Noel, R.; Liu, J.; Strachan, D. M.; Thallapally, P. K.; Cooper, A. I. Separation of Rare

- Gases and Chiral Molecules by Selective Binding in Porous Organic Cages. *Nat. Mater.* **2014**, *13*, 954–960.
- (16) Tozawa, T.; Jones, J. T. A.; Swamy, S. I.; Jiang, S.; Adams, D. J.; Shakespeare, S.; Clowes, R.; Bradshaw, D.; Hasell, T.; Chong, S. Y.; Tang, C.; Thompson, S.; Parker, J.; Trewin, A.; Bacsa, J.; Slawin, A. M. Z.; Steiner, A.; Cooper, A. I. Porous Organic Cages. *Nat. Mater.* **2009**, *8*, 973–978.
- (17) Gong, L.; Ye, Y.; Liu, Y.; Li, Y.; Bao, Z.; Xiang, S.; Zhang, Z.; Chen, B. A Microporous Hydrogen-Bonded Organic Framework for Efficient Xe/Kr Separation. ACS Appl. Mater. Interfaces 2022, 14, 19623–19628.
- (18) Lee, W.-G.; Yoon, T.-U.; Bae, Y.-S.; Kim, K. S.; Baek, S. B. Selective Separation of Xe/Kr and Adsorption of Water in a Microporous Hydrogen-bonded Organic Framework. *RSC Adv.* **2019**, *9*, 36808–36814.
- (19) Patil, R. S.; Banerjee, D.; Simon, C. M.; Atwood, J. L.; Thallapally, P. K. Noria: A Highly Xe-Selective Nanoporous Organic Solid. *Chem. Eur. J.* **2016**, 22, 12618–12623.
- (20) Miklitz, M.; Jiang, S.; Clowes, R.; Briggs, M. E.; Cooper, A. I.; Jelfs, K. E. Computational Screening of Porous Organic Molecules for Xenon/Krypton Separation. *J. Phys. Chem. C* **2017**, *121*, 15211–15222.
- (21) Lucero, J. M.; Carreon, M. A. Separation of Light Gases from Xenon over Porous Organic Cage Membranes. ACS Appl. Mater. Interfaces 2020, 12, 32182–32188.
- (22) Liu, M.; Zhang, L.; Little, M. A.; Kapil, V.; Ceriotti, M.; Yang, S.; Ding, L.; Holden, D. L.; Balderas-Xicohténcatl, R.; He, D.; Clowes, R.; Chong, S. Y.; Schütz, G.; Chen, L.; Hirscher, M.; Cooper, A. I. Barely Porous Organic Cages for Hydrogen Isotope Separation. *Science* 2019, 366, 613–620.
- (23) Hernández-Ibáñez, N.; Lee, J.-S. M.; Iniesta, J.; Leguey, V. M.; Briggs, M. E.; Cooper, A. I.; Madrid, E.; Marken, F. pH Effects on Molecular Hydrogen Storage in Porous Organic Cages Deposited onto Platinum Electrodes. *J. Electroanal. Chem.* **2018**, *819*, 46–50.
- (24) He, Y.; Xiang, S.; Chen, B. A Microporous Hydrogen-Bonded Organic Framework for Highly Selective C_2H_2/C_2H_4 Separation at Ambient Temperature. *J. Am. Chem. Soc.* **2011**, 133, 14570–14573.
- (25) Gao, J.; Cai, Y.; Qian, X.; Liu, P.; Wu, H.; Zhou, W.; Liu, D.; Li, L.; Lin, R.; Chen, B. A Microporous Hydrogen-Bonded Organic Framework for the Efficient Capture and Purification of Propylene. *Angew. Chem., Int. Ed.* **2021**, *60*, 20400–20406.
- (26) Zhang, X.; Li, L.; Wang, J.-X.; Wen, H.-M.; Krishna, R.; Wu, H.; Zhou, W.; Chen, Z.-N.; Li, B.; Qian, G.; Chen, B. Microporous Hydrogen-Bonded Organic Framework for Highly Efficient Turn-Up Fluorescent Sensing of Aniline. *J. Am. Chem. Soc.* **2020**, *142*, 633–640.
- (27) Li, P.; He, Y.; Arman, H. D.; Krishna, R.; Wang, H.; Weng, L.; Chen, B. A Microporous Six-Fold Interpenetrated Hydrogen-Bonded Organic Framework for Highly Selective Separation of C_2H_4/C_2H_6 . *Chem. Commun.* **2014**, *50*, 13081–13084.
- (28) Yang, Y.; Li, L.; Lin, R.-B.; Ye, Y.; Yao, Z.; Yang, L.; Xiang, F.; Chen, S.; Zhang, Z.; Xiang, S.; Chen, B. Ethylene/ethane Separation in a Stable Hydrogen-Bonded Organic Framework Through a Gating Mechanism. *Nat. Chem.* **2021**, *13*, 933–939.
- (29) Su, K.; Wang, W.; Du, S.; Ji, C.; Yuan, D. Efficient Ethylene Purification by a Robust Ethane-trapping Porous Organic Cage. *Nat. Commun.* **2021**, *12*, 3703.
- (30) Elbert, S. M.; Regenauer, N. I.; Schindler, D.; Zhang, W.-S.; Rominger, F.; Schröder, R. R.; Mastalerz, M. Shape-Persistent Tetrahedral [4 + 6] Boronic Ester Cages with Different Degrees of Fluoride Substitution. *Chem. Eur. J.* **2018**, *24*, 11438–11443.
- (31) Wang, W.; Su, K.; El-Sayed, E.-S. M.; Yang, M.; Yuan, D. Solvatomorphism Influence of Porous Organic Cage on C_2H_2/CO_2 Separation. ACS Appl. Mater. Interfaces 2021, 13, 24042–24050.
- (32) Li, P.; He, Y.; Zhao, Y.; Weng, L.; Wang, H.; Krishna, R.; Wu, H.; Zhou, W.; O'Keeffe, M.; Han, Y.; Chen, B. A Rod-Packing Microporous Hydrogen-Bonded Organic Framework for Highly Selective Separation of C₂H₂/CO₂ at Room Temperature. *Angew. Chem., Int. Ed.* **2014**, *54*, 574–577.

- (33) Charles, C. D.; Bloch, E. D. High-pressure Methane Storage and Selective Gas Adsorption in a Cyclohexane-Functionalised Porous Organic Cage. *Supramol. Chem.* **2019**, *31*, 508–513.
- (34) Manurung, R.; Holden, D.; Miklitz, M.; Chen, L.; Hasell, T.; Chong, S. Y.; Haranczyk, M.; Cooper, A. I.; Jelfs, K. E. Tunable Porosity through Cooperative Diffusion in a Multicomponent Porous Molecular Crystal. *J. Phys. Chem. C* **2015**, *119*, 22577–22586.
- (35) Evans, J. D.; Huang, D. M.; Hill, M. R.; Sumby, C. J.; Sholl, D. S.; Thornton, A. W.; Doonan, C. J. Molecular Design of Amorphous Porous Organic Cages for Enhanced Gas Storage. *J. Phys. Chem. C* **2015**, *119*, 7746–7754.
- (36) Burgun, A.; Valente, P.; Evans, J. D.; Huang, D. M.; Sumby, C. J.; Doonan, C. J. Endohedrally Functionalised Porous Organic Cages. *Chem. Commun.* **2016**, *52*, 8850–8853.
- (37) Atwood, J. L.; Barbour, L. J.; Jerga, A. Storage of Methane and Freon by Interstitial van der Waals Confinement. *Science* **2002**, *296*, 2367–2369.
- (38) Martínez-Ahumada, E.; He, D.; Berryman, V.; López-Olvera, A.; Hernandez, M.; Jancik, V.; Martis, V.; Vera, M. A.; Lima, E.; Parker, D. J.; Cooper, A. I.; Ibarra, I. A.; Liu, M. SO₂ Capture Using Porous Organic Cages. *Angew. Chem., Int. Ed.* **2021**, *60*, 17556–17563.
- (39) Chen, T.-H.; Popov, I.; Kaveevivitchai, W.; Chuang, Y.-C.; Chen, Y.-S.; Daugulis, O.; Jacobson, A. J.; Miljanić, O. Š. Thermally Robust and Porous Noncovalent Organic Framework with High Affinity for Fluorocarbons and CFCs. *Nat. Commun.* **2014**, *5*, 5131.
- (40) Chen, T.-H.; Popov, I.; Kaveevivitchai, W.; Chuang, Y.-C.; Chen, Y.-S.; Jacobson, A. J.; Miljanić, O. Š. Mesoporous Fluorinated Metal-organic Frameworks with Exceptional Adsorption of Fluorocarbons and CFCs. *Angew. Chem., Int. Ed.* **2015**, *54*, 13902–13906.
- (41) Chen, T.-H.; Kaveevivitchai, W.; Jacobson, A. J.; Miljanić, O. Š. Adsorption of Fluorinated Anesthetics within the Pores of a Molecular Crystal. *Chem. Commun.* **2015**, *51*, 14096–14098.
- (42) Tian, K.; Elbert, S. M.; Hu, X.; Kirschbaum, T.; Zhang, W.; Rominger, F.; Schröder, R. R.; Mastalerz, M. Highly Selective Adsorption of Perfluorinated Greenhouse Gases by Porous Organic Cages. *Adv. Mater.* **2022**, *34*, 2202290.
- (43) Hasell, T.; Miklitz, M.; Stephenson, A.; Little, M. A.; Chong, S. Y.; Clowes, R.; Chen, L.; Holden, D.; Tribello, G. A.; Jelfs, K. E.; Cooper, A. I. Porous Organic Cages for Sulfur Hexafluoride Separation. J. Am. Chem. Soc. 2016, 138, 1653–1659.
- (44) Håkansson, P.; Javed, M. A.; Komulainen, S.; Chen, L.; Holden, D.; Hasell, T.; Cooper, A.; Lantto, P.; Telkki, V.-V. NMR Relaxation and Modelling Study of the Dynamics of SF₆ and Xe in Porous Organic Cages. *Phys. Chem. Chem. Phys.* **2019**, 21, 24373–24382.
- (45) Mastalerz, M.; Schneider, M. W.; Oppel, I. M.; Presly, O. A Salicylbisimine Cage Compound with High Surface Area and Selective CO₂/CH₄ Adsorption. *Angew. Chem., Int. Ed.* **2011**, *50*, 1046–1051.
- (46) Jin, Y.; Voss, B. A.; Noble, R. D.; Zhang, W. A Shape-Persistent Organic Molecular Cage with High Selectivity for the Adsorption of CO₂ over N₂. Angew. Chem., Int. Ed. **2010**, 49, 6348–6351.
- (47) Wang, Y.; McHale, C.; Wang, X.; Chang, C.; Chuang, Y.; Kaveevivitchai, W.; Miljanić, O. Š.; Chen, T.-H. Cyclotetrabenzoin Acetate: A Macrocyclic Porous Molecular Crystal for CO₂ Separations by Pressure Swing Adsorption. *Angew. Chem., Int. Ed.* **2021**, *60*, 14931–14937.
- (48) Wang, Y.-T.; Jalife, S.; Robles, A.; Đerić, M.; Wu, J. I.; Kaveevivitchai, W.; Miljanić, O. Š.; Chen, T.-H. Efficient CO₂/CO Separation by Pressure Swing Adsorption Using an Intrinsically Nanoporous Molecular Crystal. *ACS Appl. Nano Mater.* **2022**, *5*, 14021–14026.
- (49) Yang, W.; Wang, J.; Wang, H.; Bao, Z.; Zhao, J. C.-G.; Chen, B. Highly Interpenetrated Robust Microporous Hydrogen-Bonded Organic Framework for Gas Separation. *Cryst. Growth Des.* **2017**, 17, 6132–6137.
- (50) Yang, W.; Greenaway, A.; Lin, X.; Matsuda, R.; Blake, A. J.; Wilson, C.; Lewis, W.; Hubberstey, P.; Kitagawa, S.; Champness, N. R.; Schröder, M. Exceptional Thermal Stability in a Supramolecular

- Organic Framework: Porosity and Gas Storage. J. Am. Chem. Soc. 2010, 132, 14457–14469.
- (51) Wang, H.; Li, B.; Wu, H.; Hu, T.-L.; Yao, Z.; Zhou, W.; Xiang, S.; Chen, B. A Flexible Microporous Hydrogen-Bonded Organic Framework for Gas Sorption and Separation. *J. Am. Chem. Soc.* **2015**, 137, 9963–9970.
- (52) Lü, J.; Perez-Krap, C.; Suyetin, M.; Alsmail, N. H.; Yan, Y.; Yang, S.; Lewis, W.; Bichoutskaia, E.; Tang, C. C.; Blake, A. J.; Cao, R.; Schröder, M. A Robust Binary Supramolecular Organic Framework (SOF) with High CO₂ Adsorption and Selectivity. *J. Am. Chem. Soc.* **2014**, *136*, 12828–12831.
- (53) Ma, K.; Li, P.; Xin, J. H.; Chen, Y.; Chen, Z.; Goswami, S.; Liu, X.; Kato, S.; Chen, H.; Zhang, X.; Bai, J.; Wasson, M. C.; Maldonado, R. R.; Snurr, R. Q.; Farha, O. K. Ultrastable Mesoporous Hydrogen-Bonded Organic Framework-Based Fiber Composites toward Mustard Gas Detoxification. *Cell Rep. Phys. Sci.* 2020, *1*, 100024.
- (54) Yang, W.; Li, B.; Wang, H.; Alduhaish, O.; Alfooty, K.; Zayed, M. A.; Li, P.; Arman, H. D.; Chen, B. A Microporous Porphyrin-Based Hydrogen-Bonded Organic Framework for Gas Separation. *Cryst. Growth Des.* **2015**, *15*, 2000–2004.
- (55) Song, Q.; Jiang, S.; Hasell, T.; Liu, M.; Sun, S.; Cheetham, A. K.; Sivaniah, E.; Cooper, A. I. Porous Organic Cage Thin Films and Molecular-sieving Membranes. *Adv. Mater.* **2016**, *28*, 2629–2637.
- (56) Kewley, A.; Stephenson, A.; Chen, L.; Briggs, M. E.; Hasell, T.; Cooper, A. I. Porous Organic Cages for Gas Chromatography Separations. *Chem. Mater.* **2015**, *27*, 3207–3210.
- (57) Zhang, J.-H.; Xie, S.-M.; Chen, L.; Wang, B.-J.; He, P.-G.; Yuan, L.-M. Homochiral Porous Organic Cage with High Selectivity for the Separation of Racemates in Gas Chromatography. *Anal. Chem.* **2015**, 87, 7817–7824.
- (58) Li, P.; He, Y.; Guang, J.; Weng, L.; Zhao, J. C.-G.; Xiang, S.; Chen, B. A Homochiral Microporous Hydrogen-Bonded Organic Framework for Highly Enantioselective Separation of Secondary Alcohols. *J. Am. Chem. Soc.* **2014**, *136*, 547–549.
- (59) Wang, B.; Lin, R.-B.; Zhang, Z.; Xiang, S.; Chen, B. Hydrogen-Bonded Organic Frameworks as a Tunable Platform for Functional Materials. *J. Am. Chem. Soc.* **2020**, *142*, 14399–14416.
- (60) Liu, T.; Wang, B.; He, R.; Arman, H.; Schanze, K. S.; Xiang, S.; Li, D.; Chen, B. A Novel Hydrogen-bonded Organic Framework for the Sensing of Two Representative Organic Arsenics. *Can. J. Chem.* **2020**, *98*, 352–357.
- (61) Lin, Z.-J.; Qin, J.-Y.; Zhan, X.-P.; Wu, K.; Cao, G.-J.; Chen, B. Robust Mesoporous Functional Hydrogen-Bonded Organic Framework for Hypochlorite Detection. ACS Appl. Mater. Interfaces 2022, 14, 21098–21105.
- (62) Feng, X.; Wu, J.; Liao, P.; Guo, J.; Li, Z.; Lin, R.; Chi, Z.; Zhang, J.; James, S. L. Pillararene for Fluorescence Detection of *n*-Alkane Vapours. *Mater. Chem. Front.* **2021**, *5*, 7910–7920.
- (63) Lubczyk, D.; Siering, C.; Lörgen, J.; Shifrina, Z. B.; Müllen, K.; Waldvogel, S. R. Simple and Sensitive Online Detection of Triacetone Triperoxide Explosive. *Sens. Actuators B Chem.* **2010**, *143*, 561–566.
- (64) Brutschy, M.; Schneider, M. W.; Mastalerz, M.; Waldvogel, S. R. Porous Organic Cage Compounds as Highly Potent Affinity Materials for Sensing by Quartz Crystal Microbalances. *Adv. Mater.* **2012**, *24*, 6049–6052.
- (65) Schneider, M. W.; Oppel, I. M.; Mastalerz, M. Exo-Functionalized Shape-Persistent [2 + 3] Cage Compounds: Influence of Molecular Rigidity on Formation and Permanent Porosity. *Chem. Eur. J.* **2012**, *18*, 4156–4160.
- (66) Girschikofsky, M.; Rosenberger, M.; Belle, S.; Brutschy, M.; Waldvogel, S. R.; Hellmann, R. Highly Sensitive Detection of Naphthalene in Solvent Vapor Using a Functionalized PBG Refractive Index Sensor. *Sensors* **2012**, *12*, 2018–2025.
- (67) Wessels, A.; Klöckner, B.; Siering, C.; Waldvogel, S. Practical Strategies for Stable Operation of HFF-QCM in Continuous Air Flow. *Sensors* **2013**, *13*, 12012–12029.
- (68) Brutschy, M.; Schneider, M. W.; Mastalerz, M.; Waldvogel, S. R. Direct Gravimetric Sensing of GBL by a Molecular Recognition

- Process in Organic Cage Compounds. Chem. Commun. 2013, 49, 8398.
- (69) Mastalerz, M. One-pot Synthesis of a Shape-persistent Endofunctionalised Nano-sized Adamantoid Compound. *Chem. Commun.* **2008**, 4756.
- (70) Abbott, L. J.; McDermott, A. G.; Del Regno, A.; Taylor, R. G. D.; Bezzu, C. G.; Msayib, K. J.; McKeown, N. B.; Siperstein, F. R.; Runt, J.; Colina, C. M. Characterizing the Structure of Organic Molecules of Intrinsic Microporosity by Molecular Simulations and X-ray Scattering. *J. Phys. Chem. B* **2013**, *117*, 355–364.
- (71) Prantl, E.; Kohl, B.; Ryvlin, D.; Biegger, P.; Wadepohl, H.; Rominger, F.; Bunz, U. H. F.; Mastalerz, M.; Waldvogel, S. R. Microporous Triptycene-Based Affinity Materials on Quartz Crystal Microbalances for Tracing of Illicit Compounds. *ChemPlusChem.* **2019**, *84*, 1239–1244.
- (72) Abbott, L. J.; McKeown, N. B.; Colina, C. M. Design Principles for Microporous Organic Solids from Predictive Computational Screening. *J. Mater. Chem. A* **2013**, *1*, 11950.
- (73) Ryvlin, D.; Dumele, O.; Linke, A.; Fankhauser, D.; Schweizer, W. B.; Diederich, F.; Waldvogel, S. R. Surface Pretreatment Boosts the Performance of Supramolecular Affinity Materials on Quartz Crystal Microbalances for Sensor Applications. *ChemPlusChem.* **2017**, 82, 493–497.
- (74) Karmakar, A.; Illathvalappil, R.; Anothumakkool, B.; Sen, A.; Samanta, P.; Desai, A. V.; Kurungot, S.; Ghosh, S. K. Hydrogenbonded Organic Frameworks (HOFs): A New Class of Porous Crystalline Proton-conducting Materials. *Angew. Chem., Int. Ed.* **2016**, 55, 10667–10671.
- (75) Nandi, S.; Dhavale, V. M.; Shalini, S.; Werner-Zwanziger, U.; Singh, H.; Kurungot, S.; Vaidhyanathan, R. Lithium-Assisted Proton Conduction at 150 °C in a Microporous Triazine-phenol Polymer. *Adv. Mater. Interfaces* **2015**, *2*, 1500301.
- (76) Xing, G.; Yan, T.; Das, S.; Ben, T.; Qiu, S. Synthesis of Crystalline Porous Organic Salts with High Proton Conductivity. *Angew. Chem., Int. Ed.* **2018**, *57*, 5345–5349.
- (77) Liu, M.; Chen, L.; Lewis, S.; Chong, S. Y.; Little, M. A.; Hasell, T.; Aldous, I. M.; Brown, C. M.; Smith, M. W.; Morrison, C. A.; Hardwick, L. J.; Cooper, A. I. Three-dimensional Protonic Conductivity in Porous Organic Cage Solids. *Nat. Commun.* **2016**, 7, 12750.
- (78) Yoon, M.; Suh, K.; Kim, H.; Kim, Y.; Selvapalam, N.; Kim, K. High and Highly Anisotropic Proton Conductivity in Organic Molecular Porous Materials. *Angew. Chem., Int. Ed.* **2011**, *50*, 7870–7873.
- (79) Yamada, T.; Otsubo, K.; Makiura, R.; Kitagawa, H. Designer Coordination Polymers: Dimensional Crossover Architectures and Proton Conduction. *Chem. Soc. Rev.* **2013**, *42*, *6655*.
- (80) O'Reilly, N.; Giri, N.; James, S. L. Porous Liquids. Chem. Eur. J. **2007**, 13, 3020–3025.
- (81) Giri, N.; Del Pópolo, M. G.; Melaugh, G.; Greenaway, R. L.; Rätzke, K.; Koschine, T.; Pison, L.; Gomes, M. F. C.; Cooper, A. I.; James, S. L. Liquids with Permanent Porosity. *Nature* **2015**, *527*, 216–220.
- (82) Jiang, S.; Jones, J. T. A.; Hasell, T.; Blythe, C. E.; Adams, D. J.; Trewin, A.; Cooper, A. I. Porous Organic Molecular Solids by Dynamic Covalent Scrambling. *Nat. Commun.* **2011**, *2*, 207.
- (83) Hasell, T.; Culshaw, J. L.; Chong, S. Y.; Schmidtmann, M.; Little, M. A.; Jelfs, K. E.; Pyzer-Knapp, E. O.; Shepherd, H.; Adams, D. J.; Day, G. M.; Cooper, A. I. Controlling the Crystallization of Porous Organic Cages: Molecular Analogs of Isoreticular Frameworks Using Shape-Specific Directing Solvents. *J. Am. Chem. Soc.* **2014**, *136*, 1438–1448.
- (84) Greenaway, R. L.; Holden, D.; Eden, E. G. B.; Stephenson, A.; Yong, C. W.; Bennison, M. J.; Hasell, T.; Briggs, M. E.; James, S. L.; Cooper, A. I. Understanding Gas Capacity, Guest Selectivity, and Diffusion in Porous Liquids. *Chem. Sci.* **2017**, *8*, 2640–2651.
- (85) Kearsey, R. J.; Alston, B. M.; Briggs, M. E.; Greenaway, R. L.; Cooper, A. I. Accelerated Robotic Discovery of Type II Porous Liquids. *Chem. Sci.* **2019**, *10*, 9454–9465.

- (86) Jie, K.; Onishi, N.; Schott, J. A.; Popovs, I.; Jiang, D.; Mahurin, S.; Dai, S. Transforming Porous Organic Cages into Porous Ionic Liquids via a Supramolecular Complexation Strategy. *Angew. Chem., Int. Ed.* **2020**, *59*, 2268–2272.
- (87) Melaugh, G.; Giri, N.; Davidson, C. E.; James, S. L.; Del Pópolo, M. G. Designing and Understanding Permanent Microporosity in Liquids. *Phys. Chem. Chem. Phys.* **2014**, *16*, 9422–9431.
- (88) Hemming, E. B.; Masters, A. F.; Maschmeyer, T. Exploring Opportunities for Platinum Nanoparticles Encapsulated in Porous Liquids as Hydrogenation Catalysts. *Chem. Eur. J.* **2020**, *26*, 7059–7064
- (89) Wang, Y.; Sun, Y.; Bian, H.; Zhu, L.; Xia, D.; Wang, H. Cyclodextrin Porous Liquid Materials for Efficient Chiral Recognition and Separation of Nucleosides. *ACS Appl. Mater. Interfaces* **2020**, *12*, 45916–45928.

□ Recommended by ACS

Polymer-Coated Covalent Organic Frameworks as Porous Liquids for Gas Storage

Rachel E. Mow, Wade A. Braunecker, et al.

JANUARY 19, 2024

CHEMISTRY OF MATERIALS

READ 🗹

Microporous Polyelectrolyte Complexes by Hydroplastic Foaming

Zi-Xuan Liang, Xia-Chao Chen, et al.

JANUARY 09, 2024

LANGMUIR

READ 🗹

Designing and Molding Covalent Organic Frameworks for Separation Applications

Sa Wang, Zhenjie Zhang, et al.

OCTOBER 06, 2023

ACCOUNTS OF MATERIALS RESEARCH

READ 🗹

Enhancing Structure-Property Relationships in Porous Materials through Transfer Learning and Cross-Material Few-Shot Learning

Hyunsoo Park, Jihan Kim, et al.

NOVEMBER 20, 2023

ACS APPLIED MATERIALS & INTERFACES

READ 🗹

Get More Suggestions >